that cholesterol regulates the localization of mature NEP in lipid rafts, where the substrate Aβ accumulates but apparently does not modulate the protease activity of NEP.

## MATERIALS AND METHODS

### Vectors and Constructs

Human neprilysin, NEP WT, was inserted into the pcDNA3.1-3 × FLAG vector (Invitrogen, Carlsbad, CA), thereby fusing triplet tandem repeats of FLAG tag to its N-terminus. The expression product of this construct will be referred to as FLAG-NEP WT. NEP E584V, carrying a catalytically inactive mutant E584V, and NEP E403C, carrying a homodimerization mutant, were subcloned into the pcDNA3.1-3 × FLAG vector, yielding FLAG-NEP E584V and FLAG-NEP E403C, respectively.

### Antibodies

The following antibodies were purchased: anti-FLAG M2 (Sigma, St. Louis, MO); antiflotillin-1 and anticalnexin (BD Transduction Laboratories, Lexington, KY); anti-monoclonal NEP (Leica Microsystems); and HRP-conjugated anti-mouse IgG (Cell Signaling Technology, Beverly, MA).

### Cell Culture and Transfection

HEK293 cells were cultured in DMEM (Sigma) supplemented with 10% fetal bovine serum (Sigma). They were maintained at 37°C in an atmosphere containing 5% $CO_2$ in a tissue culture incubator. DNA transfection was performed by lipofection with FuGENE 6 Transfection Reagent (Roche, Indianapolis, IN) when cells were 50% confluent. Then, 24 hr later, cells were harvested or used in assays.

### Isolation of the Membrane Fraction

Cells were dissolved in TBS (0.1 M Tris-HCl, pH 8.0, 150 mM NaCl) containing Complete, EDTA-free protease inhibitor (Roche) and 0.7 μg/ml pepstatin A (Sigma) and disrupted by passage 20 times through a 21-G needle. The cell sample was then centrifuged (2,000 rpm, 2 min, 4°C). The resulting supernatant was then centrifuged again (49,000 rpm, 30 min, 4°C; Optima MAX-E ultracentrifuge; Beckman Coulter). The pellet formed was dissolved in TBS containing Complete, EDTA-free protease inhibitors, 0.7 μg/ml pepstatin A, and 1% Triton X-100; incubated on ice for 1 hr; and ultracentrifuged again. The resulting supernatant will be referred to as the *membrane fraction.*

### Enzymatic Deglycosylation

The membrane fraction was solubilized with 1% Triton X-100 and then deglycosylated through treatment with the following: 1) endoglycosidase H (endo H; BioLabs), according to the manufacturer's instructions, and 2) 1 U N-glycosidase F (Endo F; Roche) per 45 μg of protein. The membrane fraction was denatured by boiling for 3 min in 1% SDS and 2-mercaptoethanol (ME), suspended in a reaction buffer (50 mM EDTA, 1% 2-ME, 0.5% Triton X-100, 0.1% SDS, 1 U N-glycosidase F) containing Complete, EDTA-free protease inhibitors and 0.7 μg/ml pepstatin A and incubated at 37°C overnight.

### Isolation of Lipid Rafts by Sucrose Density Gradient Centrifugation

Cells were lysed on ice in MBS buffer (25 mM MES, pH 6.5, 150 mM NaCl) containing 1% Triton X-100, Complete, EDTA-free protease inhibitors, and 0.7 μg/ml pepstatin A. Cell disruption was achieved by passing the lysate 10 times through a 21-G needle and then 20 times through a 27-G needle. The lysate was incubated at 4°C for 30 min, and an equal amount of 80% sucrose was then added to it. The sample and sucrose buffer, containing 5–40% sucrose, were sequentially loaded to the bottom of a tube and then centrifuged (36,000 rpm, 18 hr, 4°C; CP 70 WX ultracentrifuge; Hitachi). Fractions were collected from the top to the bottom. Equal volumes of these samples were analyzed by Western blotting.

### Methyl-β-Cyclodextrin Treatment

HEK293 cells overexpressing FLAG NEP-WT were washed with PBS, treated with 10 mM methyl-β-cyclodextrin (MβCD; Trappsol) for 20 min in a $CO_2$ incubator at 37°C, and collected. Lipid rafts fractions were treated with 50 mM MβCD on ice for 1 hr, dissolved in a double volume of TBS containing Complete, EDTA-free protease inhibitors and 0.7 μg/ml pepstatin A, and centrifuged (49,000 rpm, 1 hr, 4°C). The supernatants were removed and the pellets dissolved in TBS.

### Western Blotting

Equal amounts of protein samples were separated by SDS-PAGE or Blue Native-PAGE and transferred to Immobilon-P PVDF membranes (Millipore, Billerica, MA). In the case of Blue Native-PAGE, the membranes were washed and destained using methanol. The membranes were soaked in PBS containing 5% nonfat dried milk and 0.05% Tween for 1 hr and then incubated overnight at 4°C with primary antibodies diluted in PBS containing 0.05% Tween, 0.1% BSA, and 1 mM $NaN_3$. After washing, the membranes were incubated with HRP-conjugated secondary antibody for 1 hr. Antigen–antibody complexes were detected by enhanced chemiluminescence using a LAS-3000 Luminescent Image Analyzer (Fujifilm). Signals were quantified in MultiGauge software (version 2.3; Fujifilm).

### Assay of NEP-Dependent Neutral Endopeptidase Activity

NEP activity was measured in vitro by incubation at 37°C for 1 hr in 100 mM MES (pH 6.8) containing Complete, EDTA-free protease inhibitors, 10 μM Z-Leu-Leu-Leu-H, and as a substrate 50 μM Z-Ala-Ala-Leu-*p*-nitroanilide (ZALL-*p*-NA; Peptide Institute), in the presence or absence of 10 μM thiorphan, a specific inhibitor of NEP.

### Interaction of NEP With Various Lipids

Lipid-spotted membrane (P-6002; Echelon Biosciences) was treated with TBS containing 1% skim milk and gently

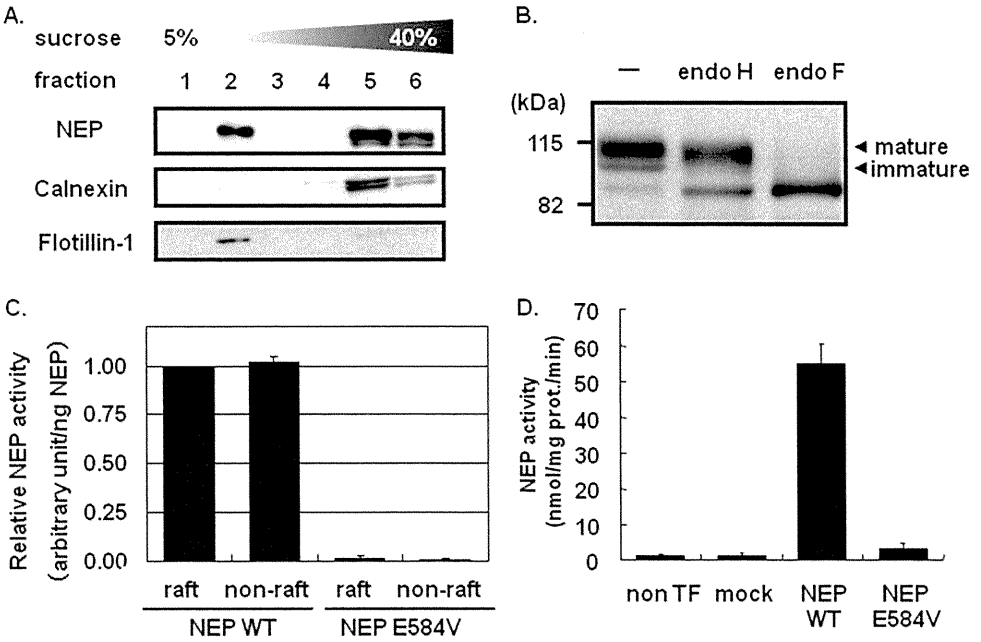


Fig. 1. NEP localization and activity in lipid rafts. **A:** Western blot analysis of lipid rafts fractionated from HEK293 cells overexpressing FLAG-NEP WT by a sucrose density-gradient centrifugation method. An anti-FLAG antibody was used to detect NEP. Lipid rafts were detected using an antibody raised against the raft marker flotillin-1. Nonlipid rafts (fraction 5) were detected using an antibody raised against the nonraft marker calnexin. **B:** Deglycosylation of the membrane fraction prepared from HEK293 cells overexpressing FLAG-NEP WT. The membrane fraction was treated with endoglycosidase H (endo H) and endoglycosidase F (endo F) or left untreated as a control (–), and then analyzed by Western blotting with an anti-FLAG antibody. **C:** Comparison of the specific enzymatic activity of the mature form NEP in lipid rafts (fraction 2) and nonlipid rafts (fraction 5), as assessed by *p*-NA peptide assay. Values represent the mean ± SD of three experiments. **D:** Neprilysin-dependent neutral endopeptidase activity in membrane fractions prepared from nontransfected HEK293 cells (non-TF) and cells transfected with vector (mock), FLAG-NEP WT (NEP WT) or the catalytically inactive mutant FLAG-NEP E584V. Values represent the mean ± SD of three experiments.

agitated for 1 hr at room temperature. SH-SY5Y neuronal cells were fractionated by sucrose density gradient centrifugation as shown previously, and each fraction was added to an equal volume of TBS containing protease inhibitor cocktail. After centrifugation at 49,000 rpm for 1 hr, the precipitate was dissolved in TBS containing protease inhibitor cocktail and incubated with the P-6002 membrane for 1 hr at room temperature. After incubation, the membrane was washed with TBS containing 0.1% Tween three times and incubated with anti-NEP monoclonal antibody diluted 1:2,000 for 1 hr at room temperature. The bound NEP was detected with an ECL advance kit (GE Healthcare, Amersham, United Kingdom).

## RESULTS

### Localization and Peptidase Activity of NEP in Lipid Rafts

To evaluate the peptidase activity of NEP in lipid rafts, we fractionated lipid rafts by sucrose density gradient centrifugation. We analyzed the localization of membrane-bound NEP extracted from HEK293 cells overexpressing FLAG-NEP WT. A raft marker, flotillin-1, was detected in fraction 2 and a nonraft marker, calnexin, in fractions 5 and 6 (Fig. 1A). FLAG-NEP was detected as a single band in fraction 2 and doublet bands in fractions 5 and 6. To distinguish these doublet bands, we deglycosylated the membrane fraction by treating it with endoglycosidase H (endo H) and endoglycosidase F (endo F; Fig. 1B). Although the upper band, the mature form, was resistant to endo H treatment, the lower band was deglycosylated by endo H. We will refer to the latter as the *immature form* of NEP. Resistance to endo H is acquired on transport of the protein to the Golgi apparatus, and this glycosylation is important for the catalytic activity of NEP (Lafrance et al., 1994). We compared the specific enzymatic activity of the mature form of NEP in lipid rafts (fraction 2) and nonlipid rafts (fraction 5); the contents of mature NEP were equalized by densitometric measurement of mature NEP levels after immunoblotting with an anti-FLAG antibody. The NEP activities of fractions 2 and 5, as assessed by *p*-NA peptide assay, were comparable (Fig. 1C). In this assay, catalytically inactive NEP E584V was used as a negative control (Fig. 1D).

### Localization of NEP in Lipid Rafts Is Dependent on Cholesterol

Only mature NEP was detected in lipid rafts (Fig. 1A). We thus hypothesized that cholesterol in lipid rafts regulated the localization of mature NEP. To test this, we depleted HEK293 cells overexpressing FLAG-NEP

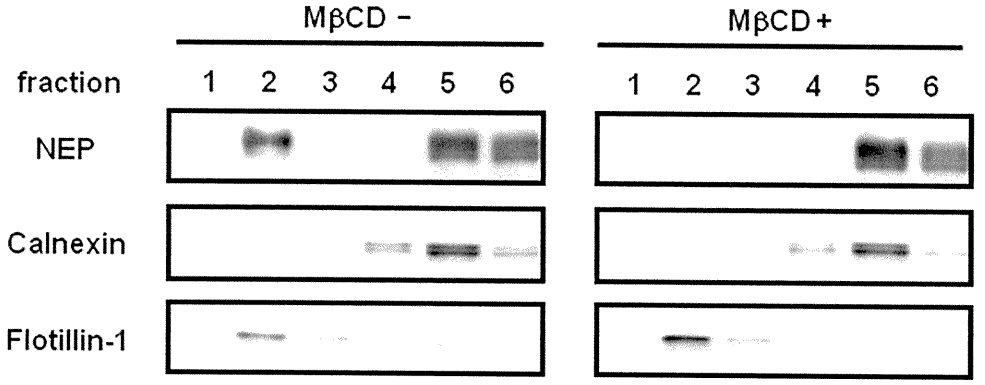


Fig. 2. Delocalization of NEP from lipid rafts in cells treated with MβCD. HEK293 cells overexpressing FLAG-NEP WT were treated with methyl-β-cyclodextrin (MβCD; +) or left untreated (–), and lipid rafts were fractionated as described in Materials and Methods.

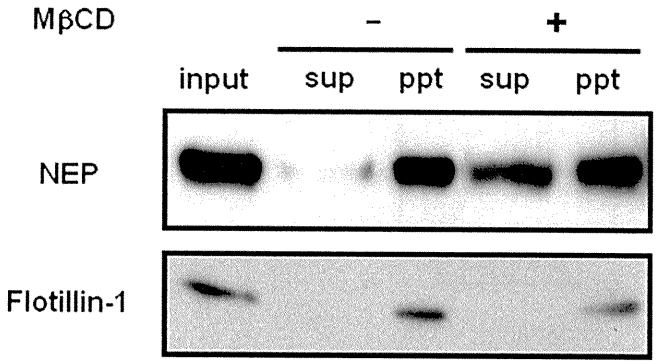


Fig. 3. Delocalization of NEP from fractionated lipid rafts after MβCD treatment. The lipid raft fraction, isolated from HEK293 cells overexpressing FLAG-NEP WT, was treated with (+) MβCD or left untreated (–) and separated into a supernatant (Sup) and a pellet (Ppt) by ultracentrifugation. The distribution of NEP was determined by Western blotting with an anti-FLAG antibody.

WT of cholesterol by treating them with 10 mM methyl-β-cyclodextrin (MβCD) for 20 min, and then fractionated the lipid rafts. More than 50% of cholesterol can be depleted from HEK293 cells by this treatment (Kojro et al., 2001). NEP became delocalized from lipid rafts following MβCD treatment, although flotillin-1 remained associated with them (Fig. 2).

We confirmed that the in vitro depletion of cholesterol from the lipid rafts fraction caused the delocalization of NEP from lipid rafts. We treated the fractionated lipid rafts with 50 mM MβCD for 1 hr at 4°C and separated them into supernatants and pellets by ultracentrifugation (Fig. 3). NEP and flotillin-1, associated with lipid rafts, were detected, as expected, in the pellets formed from lipid rafts not treated with MβCD. However, some of the NEP associated with lipid rafts was detected in supernatants prepared from lipid rafts treated with MβCD treatment. Flotillin-1 remained exclusively in the pellets, suggesting that flotillin-1 was not associated with choresterol.

## Localization of NEP in Lipid Rafts Is Enhanced by Its Dimerization

To understand better the mechanism of NEP localization in lipid rafts, we investigated whether NEP dimerization facilitated the assembly of the enzyme in lipid rafts. We lysed HEK293 cells overexpressing FLAG-NEP WT in buffers containing different detergents and then analyzed NEP protein complexes by Blue Native-PAGE. Although NEP complexes were dissociated by NP-40 and Triton X-100, the 300-kDa complexes were resistant to treatment with DDM and digitonin (Fig. 4A). Next, we investigated the effect of dimerization on the localization of NEP in lipid rafts. It has been reported that rabbit NEP carrying an E403C mutation forms a covalent homodimer (Hoang et al., 1997). We introduced this mutation into human NEP and assessed its effect on the localization of NEP in lipid rafts. FLAG-NEP WT and FLAG-NEP E403C were detected as single 120-kDa bands after their separation by SDS-PAGE under reducing conditions (Fig. 4B). A 250-kDa FLAG-NEP E403C homodimer was detected under nonreducing conditions (Fig. 4B). These results indicate that, as in rabbit NEP, the E403C mutation caused human NEP to form of a covalent homodimer. Interestingly, although NEP WT complexes (Fig. 4A,C) were not resistant to Triton X-100, the NEP E403C mutant was resistant to Triton X-100 and formed a disulfide-bonded complex the same size as the NEP WT complex. Although we cannot exclude the possibility that the complex includes other proteins, the 300-kDa complex (Fig. 4A,C) appears to represent a covalent NEP homodimer.

Next, we compared the localization of mature forms of NEP WT and NEP E403C in lipid rafts. The ratio of the amount of mature NEP localized in lipid rafts to the total amount of mature NEP was 1.3 times higher in HEK293 cells overexpressing homodimeric mutant NEP E403C (47.7%) than in those expressing NEP WT (35.7%; Fig. 4D). These results demonstrate that the localization of NEP in lipid rafts was enhanced by its dimerization.

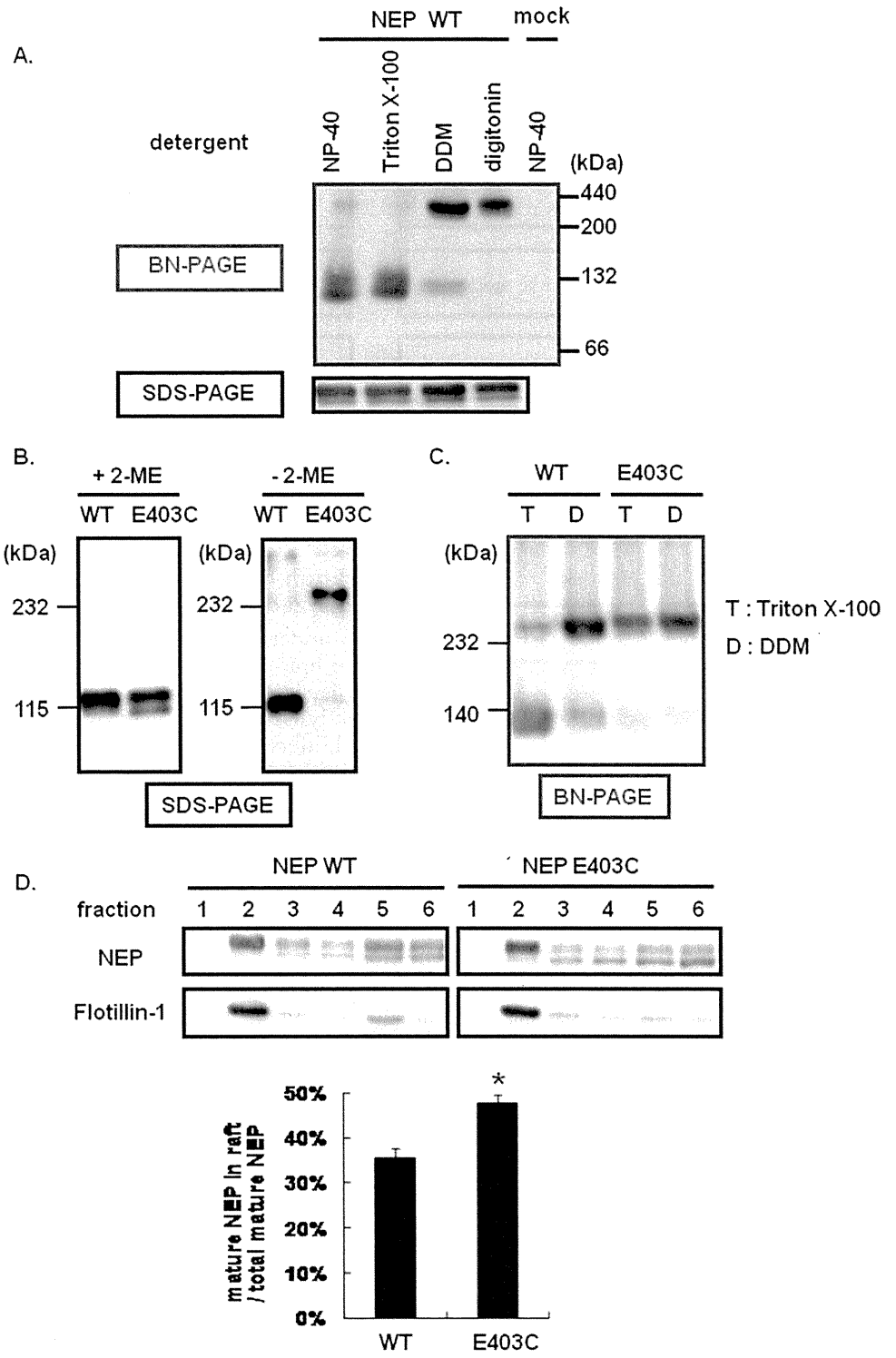


Fig. 4. Dimerization and localization of human NEP E403C in lipid rafts. **A:** Membrane fractions prepared from HEK293 cells overexpressing FLAG-NEP WT (NEP WT) or vector (mock) were dissolved in buffer containing detergents, such as NP-40, Triton X-100, DDM, and digitonin (all at a concentration of 1%). NEP complexes were analyzed by Blue Native-PAGE (BN-PAGE) or SDS-PAGE, followed by Western blotting with an anti-FLAG antibody. **B:** Membrane fractions obtained from HEK293 cells overexpressing FLAG-NEP WT (WT) or FLAG-NEP E403C (E403C) were analyzed by SDS-PAGE, performed with (**left**) or without (**right**) 2-ME. **C:** Membrane fractions obtained from HEK293 cells overexpressing FLAG-NEP WT (WT) or FLAG-NEP E403C (E403C) were dissolved in buffer containing 1% Triton X-100 (T) or 1% of DDM (D). The resulting lysates were analyzed by Blue Native-PAGE (BN-PAGE) and Western blotting with an anti-FLAG antibody. **D:** Effect of the E403C mutation on the distribution of NEP in lipid rafts. Lipid rafts from HEK293 cells overexpressing FLAG-NEP WT (NEP WT) or FLAG-NEP E403C (NEP E403C) were fractionated by sucrose density-gradient centrifugation and analyzed by Western blotting with an anti-FLAG antibody. The ratio of the amount of mature NEP localized in lipid rafts to the total amount of mature NEP was determined by densitometric measurement of protein bands corresponding to the mature form of NEP. Values represent the mean ± SD of three experiments. Statistical analysis was performed using a two-tailed Student's *t*-test. $*P < 0.05$ was considered to indicate statistical significance (bottom graph).

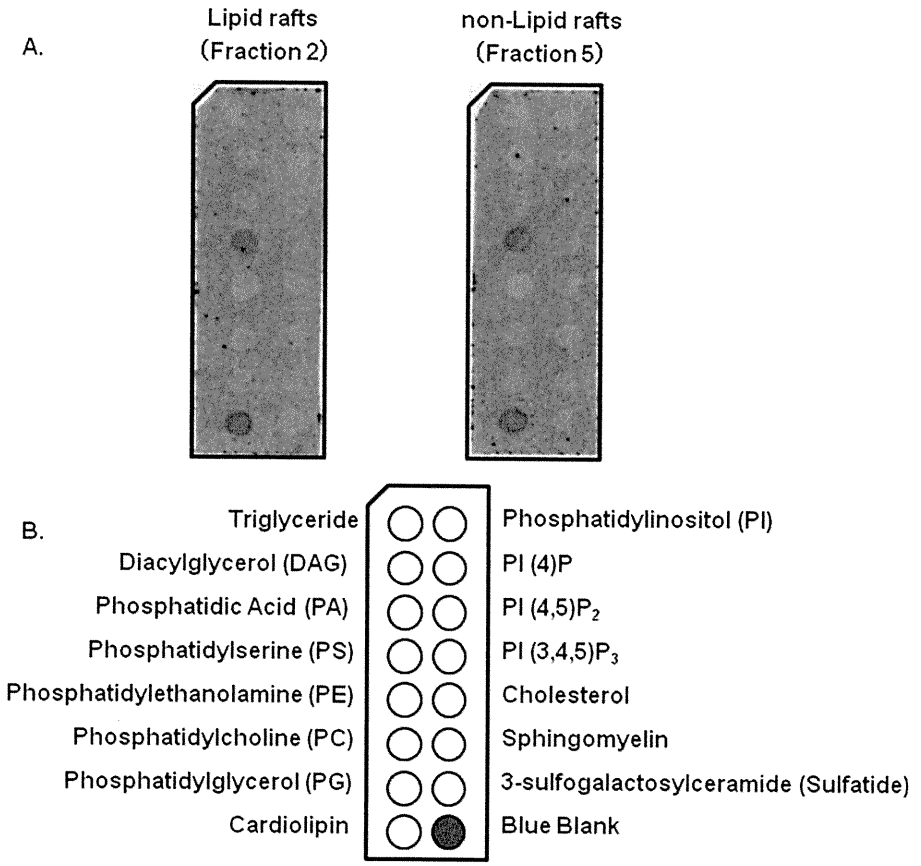


Fig. 5. Interaction of NEP with various lipids. Lipid-attached membrane was treated with sucrose density fractions of SH-SY5Y neuronal cells. After incubation and washing, the membrane was incubated with anti-NEP monoclonal antibody as described in Materials and Methods. The bound NEP was detected by ECL advance. **A:** ECL results. **B:** Lipids attached to the membrane.

### Direct Inteaction of NEP With Lipids

The results described above suggest that NEP is localized in lipid rafts, possibly by its direct association with cholesterol. Finally, interaction of NEP with lipids was investigated by using lipid-spotted P-6002 membrane. Fractionated rafts (fraction 2 in Fig. 1A) and nonrafts fractions (fraction 5 in Fig. 1A) were concentrated by ultracentrifugation and incubated with lipids. After washing of the P-6002 membrane, lipid-bound NEP was detected by the specific antibody. Unexpectedly, NEP both in lipid rafts and in nonrafts fractions interacted with phosphatidylserine and cardiolipin but not with cholesterol (Fig. 5).

## DISCUSSION

In this study, we found that only the mature form of NEP, glycosylated in the Golgi, and not the immature form, residing in the ER, was localized in lipid rafts (Fig. 1A,B). This indicates that complete glycosylation is required for the association of NEP with lipid rafts. Two possible explanations for this were considered. One is that maturation may be necessary for NEP to bind to a carrier protein such as a glycosylphosphatidylinositol (GPI)-anchored protein. The other is that a small conformational change caused by maturation increases the affinity of NEP for molecules found in lipid rafts, such as sphingolipids and cholesterol. With regard to the former, there have been several reports concerning carrier proteins. One study found that, when the transmembrane and C-terminal domains of BACE1 were replaced with a GPI anchor signal sequence, it was translocated to lipid rafts (Cordy et al., 2003). Another study found that the addition of the N-terminal domain of growth-associated protein 43 (GAP43) to the N-terminus of NEP increased the amount of NEP present in lipid rafts by 1.3-fold (Hama et al., 2004). With regard to the latter possible explanation, we found evidence that the localization of the mature form of NEP in lipid rafts was dependent on the content of cholesterol (Figs. 2, 3). Interestingly, although NEP was completely delocalized by cholesterol depletion, flotillin-1, a lipid raft marker, was not delocalized from lipid rafts by treatment with MβCD (Fig. 2). In this regard, flotillin-1 has been reported to be enriched in detergent-resistant microdomains that are MβCD resistant, although the mechanism

remains to be investigated (Rajendran et al., 2003). Moreover, to examine whether the delocalization of NEP from lipid rafts was caused by its direct association with cholesterol, we extracted lipid raft membranes and treated them with MβCD in vitro (Fig. 3). Consistently with the results presented in Figure 2, NEP was delocalized from lipid rafts membrane by cholesterol depletion, although not completely so (Fig. 3). The difference in the efficiency of NEP delocalization between cell and cell-free systems may be caused by the different conditions used (reaction temperature, membrane state, effects of ultracentrifugation). We conclude that the localization of mature NEP in lipid rafts depends on their cholesterol content.

We investigated the direct association of NEP with pure phospholipids and cholesterol (Fig. 5). Both NEP in rafts and nonrafts directly interacted with phosphatidylserine and cardiolipin. Cardiolipin is a major phospholipid of inner membrane of mammalian mitochondria, so phosphatidylserine might be the major interactor of NEP in lipid rafts. Moreover, immunocytochemical analysis showed that the clustered localization of endogenous NEP in SH-SY5Y cells became dispersed after MβCD treatment (Supp. Info. Fig. 1). Therefore, we conclude that NEP directly associated with phosphatidylserine in cholesterol-rich lipid rafts and MβCD-induced cholesterol depletion triggers the destruction of lipid composition and releases the NEP from rafts. However, the protease activities of mature NEP were unexpectedly comparable in lipid raft and nonlipid raft fractions, as assessed by *p*-NA peptide assay. It is possible that the fractionated lipid rafts did not reflect intracellular conditions (Pike, 2004). However, this result suggests that the association with lipid rafts does not itself modify the protease activity of NEP.

Considering the localization of Aβ in lipid rafts through association with cholesterol (Kakio et al., 2002), we hypothesized that the localization of mature NEP in lipid rafts facilitated its association with Aβ and thereby altered Aβ degradation. Recent studies have shown that lipid raft-dependent endocytosis is the predominant Aβ uptake mechanism (Lai and McLaurin, 2011), that there are correlations between memory deficits and intracellular Aβ levels in several mouse AD models (Billings et al., 2005; Knobloch et al., 2007; Bayer and Wirths, 2008), and that intracellular Aβ level correlates with extracellular amyloid deposition (Yang et al., 2011). Thus, it seems reasonable to conclude that NEP is localized and active in lipid rafts. Indeed, NEP is detected primarily in presynapses and on or around axons in the hippocampal formation (Fukami et al., 2002), and presynaptic NEP efficiently degrades Aβ (Iwata et al., 2004). Considering these findings, together with the fact that the ϵ4 allele of apolipoprotein E (apoE) is a risk factor in nonfamilial AD (Kim et al., 2009), we suggest that cholesterol, overloaded by aging or a high-fat diet, enlarges the area occupied by lipid rafts, thereby decreasing the likelihood of NEP and Aβ coming into contact with each other. As a result, Aβ becomes more abundant, oligomerizes, and causes memory deficits. However, it should be noted that cholesterol itself is a crucial contributor to synaptic structure and function. It has been reported that brain-derived neurotrophic factor (BDNF)-dependent cholesterol biosynthesis plays an important role in synapse development (Suzuki et al., 2007). It would therefore be important to maintain normal cholesterol metabolism during AD therapy.

We further investigated the effects of dimerization on the localization of NEP in lipid rafts. We introduced the E403C mutation into human NEP for the first time. The mutation was originally discovered in rabbit NEP, in which it causes the formation of a covalent homodimer (rabbit NEP normally exists as a monomer). Our results show that human NEP E403C, like rabbit NEP E403C, forms a covalent homodimer. In contrast, human NEP WT, like porcine NEP WT (Kenny et al., 1983), forms a noncovalent homodimer (Fig. 4A,B). Moreover, the noncovalent human NEP WT homodimer, though not resistant to NP-40 or Triton X-100, was resistant to DDM and digitonin. DDM and digitonin dissolve proteins modestly, so the complex remained intact after treatment with these detergents. Interestingly, the localization of mature NEP to lipid rafts was enhanced by its homodimerization (Fig. 4D). With regard to the endopeptidase activity of NEP E403C, Vmax/Km for this mutant was decreased by 50% compared with that for wild-type by using either [D-Ala$^2$, Leu$^5$] enkephalin or Suc-Ala-Ala-Leu-NH-Np as a substrate (Hoang et al., 1997). Although the NEP E403C mutant seems to be artificial and to have no physiological significance, these results imply that the protease activity of NEP might be modulated by its dimerization.

In conclusion, we have shown that cholesterol regulates the localization of mature NEP in lipid rafts, where its substrate, Aβ, accumulates. Cholesterol does not, however, modulate the protease activity of NEP.

## ACKNOWLEDGMENTS

We thank Dr. Nobuhisa Iwata (Nagasaki University) for providing the protocol for the assay of neprilysin-dependent neutral endopeptidase activity.

## REFERENCES

Angelisova P, Drbal K, Horejsi V, Cerny J. 1999. Association of CD10/neutral endopeptidase 24.11 with membrane microdomains rich in glycosylphosphatidylinositol-anchored proteins and Lyn kinase. Blood 93:1437–1439.

Bayer TA, Wirths O. 2008. Review on the APP/PS1KI mouse model: intraneuronal Abeta accumulation triggers axonopathy, neuron loss and working memory impairment. Genes Brain Behav 7(Suppl 1):6–11.

Billings LM, Oddo S, Green KN, McGaugh JL, LaFerla FM. 2005. Intraneuronal Abeta causes the onset of early Alzheimer's disease-related cognitive deficits in transgenic mice. Neuron 45:675–688.

Cordy JM, Hussain I, Dingwall C, Hooper NM, Turner AJ. 2003. Exclusively targeting beta-secretase to lipid rafts by GPI-anchor addition up-regulates beta-site processing of the amyloid precursor protein. Proc Natl Acad Sci U S A 100:11735–11740.

Fukami S, Watanabe K, Iwata N, Haraoka J, Lu B, Gerard NP, Gerard C, Fraser P, Westaway D, St. George-Hyslop P, Saido TC. 2002.

Abeta-degrading endopeptidase, neprilysin, in mouse brain: synaptic and axonal localization inversely correlating with Abeta pathology. Neuroscience research 43:39–56.

Hama E, Shirotani K, Iwata N, Saido TC. 2004. Effects of neprilysin chimeric proteins targeted to subcellular compartments on amyloid beta peptide clearance in primary neurons. J Biol Chem 279:30259–30264.

Hardy JA, Higgins GA. 1992. Alzheimer's disease: the amyloid cascade hypothesis. Science 256:184–185.

Hellstrom-Lindahl E, Ravid R, Nordberg A. 2008. Age-dependent decline of neprilysin in Alzheimer's disease and normal brain: inverse correlation with A beta levels. Neurobiol Aging 29:210–221.

Hoang MV, Sansom CE, Turner AJ. 1997. Mutagenesis of Glu403 to Cys in rabbit neutral endopeptidase-24.11 (neprilysin) creates a disulphide-linked homodimer: analogy with endothelin-converting enzyme. Biochem J 327:925–929.

Iwata N, Tsubuki S, Takaki Y, Shirotani K, Lu B, Gerard NP, Gerard C, Hama E, Lee HJ, Saido TC. 2001. Metabolic regulation of brain Abeta by neprilysin. Science 292:1550–1552.

Iwata N, Takaki Y, Fukami S, Tsubuki S, Saido TC. 2002. Region-specific reduction of A beta-degrading endopeptidase, neprilysin, in mouse hippocampus upon aging. J Neurosci Res 70:493–500.

Iwata N, Mizukami H, Shirotani K, Takaki Y, Muramatsu S, Lu B, Gerard NP, Gerard C, Ozawa K, Saido TC. 2004. Presynaptic localization of neprilysin contributes to efficient clearance of amyloid-beta peptide in mouse brain. J Neurosci 24:991–998.

Kakio A, Nishimoto S, Yanagisawa K, Kozutsumi Y, Matsuzaki K. 2002. Interactions of amyloid beta-protein with various gangliosides in raft-like membranes: importance of GM1 ganglioside-bound form as an endogenous seed for Alzheimer amyloid. Biochemistry 41:7385–7390.

Kanemitsu H, Tomiyama T, Mori H. 2003. Human neprilysin is capable of degrading amyloid beta peptide not only in the monomeric form but also the pathological oligomeric form. Neurosci Lett 350:113–116.

Kawarabayashi T, Shoji M, Younkin LH, Wen-Lang L, Dickson DW, Murakami T, Matsubara E, Abe K, Ashe KH, Younkin SG. 2004. Dimeric amyloid beta protein rapidly accumulates in lipid rafts followed by apolipoprotein E and phosphorylated tau accumulation in the Tg2576 mouse model of Alzheimer's disease. J Neurosci 24:3801–3809.

Kenny AJ, Fulcher IS, McGill KA, Kershaw D. 1983. Proteins of the kidney microvillar membrane. Reconstitution of endopeptidase in liposomes shows that it is a short-stalked protein. Biochem J 211:755–762.

Kim J, Basak JM, Holtzman DM. 2009. The role of apolipoprotein E in Alzheimer's disease. Neuron 63:287–303.

Knobloch M, Konietzko U, Krebs DC, Nitsch RM. 2007. Intracellular Abeta and cognitive deficits precede beta-amyloid deposition in transgenic arcAbeta mice. Neurobiol Aging 28:1297–1306.

Kojro E, Gimpl G, Lammich S, Marz W, Fahrenholz F. 2001. Low cholesterol stimulates the nonamyloidogenic pathway by its effect on the alpha-secretase ADAM 10. Proc Natl Acad Sci U S A 98:5815–5820.

Lafrance MH, Vezina C, Wang Q, Boileau G, Crine P, Lemay G. 1994. Role of glycosylation in transport and enzymic activity of neutral endopeptidase-24.11. Biochem J 302:451–454.

Lai AY, McLaurin J. 2011. Mechanisms of amyloid-beta peptide uptake by neurons: the role of lipid rafts and lipid raft-associated proteins. Int J Alzheimers Dis 2011:548380.

Matsuzaki K, Noguch T, Wakabayashi M, Ikeda K, Okada T, Ohashi Y, Hoshino M, Naiki H. 2007. Inhibitors of amyloid beta-protein aggregation mediated by GM1-containing raft-like membranes. Biochim Biophys Acta 1768:122–130.

Pike LJ. 2004. Lipid rafts: heterogeneity on the high seas. Biochem J 378:281–292.

Pike LJ. 2006. Rafts defined: a report on the Keystone Symposium on Lipid Rafts and Cell Function. J Lipid Res 47:1597–1598.

Rajendran L, Masilamani M, Solomon S, Tikkanen R, Stuermer CA, Plattner H, Illges H. 2003. Asymmetric localization of flotillins/reggies in preassembled platforms confers inherent polarity to hematopoietic cells. Proc Natl Acad Sci U S A 100:8241–8246.

Riemann D, Hansen GH, Niels-Christiansen L, Thorsen E, Immerdal L, Santos AN, Kehlen A, Langner J, Danielsen EM. 2001. Caveolae/lipid rafts in fibroblast-like synoviocytes: ectopeptidase-rich membrane microdomains. Biochem J 354:47–55.

Selkoe DJ. 2002. Alzheimer's disease is a synaptic failure. Science 298:789–791.

Suzuki S, Kiyosue K, Hazama S, Ogura A, Kashihara M, Hara T, Koshimizu H, Kojima M. 2007. Brain-derived neurotrophic factor regulates cholesterol metabolism for synapse development. J Neurosci 27:6417–6427.

von Tresckow B, Kallen KJ, von Strandmann EP, Borchmann P, Lange H, Engert A, Hansen HP. 2004. Depletion of cellular cholesterol and lipid rafts increases shedding of CD30. J Immunol 172:4324–4331.

Wada S, Morishima-Kawashima M, Qi Y, Misono H, Shimada Y, Ohno-Iwashita Y, Ihara Y. 2003. Gamma-secretase activity is present in rafts but is not cholesterol-dependent. Biochemistry 42:13977–13986.

Yang DS, Stavrides P, Mohan PS, Kaushik S, Kumar A, Ohno M, Schmidt SD, Wesson D, Bandyopadhyay U, Jiang Y, Pawlik M, Peterhoff CM, Yang AJ, Wilson DA, St. George-Hyslop P, Westaway D, Mathews PM, Levy E, Cuervo AM, Nixon RA. 2011. Reversal of autophagy dysfunction in the TgCRND8 mouse model of Alzheimer's disease ameliorates amyloid pathologies and memory deficits. Brain 134:258–277.

Biochemical and Biophysical Research Communications 409 (2011) 64–69

Contents lists available at ScienceDirect

Biochemical and Biophysical Research Communications

journal homepage: www.elsevier.com/locate/ybbrc

# Alternative splicing of *PDLIM3/ALP*, for α-actinin-associated LIM protein 3, is aberrant in persons with myotonic dystrophy

Natsumi Ohsawa [a], Michinori Koebis [a], Satoshi Suo [a], Ichizo Nishino [b], Shoichi Ishiura [a,*]

[a] Department of Life Sciences, Graduate School of Arts and Sciences, The University of Tokyo, 3-8-1 Komaba, Meguro-ku, Tokyo 153-8902, Japan
[b] National Institute of Neuroscience, National Center of Neurology and Psychiatry (NCNP), 4-1-1 Ogawahigashi, Kodaira, Tokyo 187-8502, Japan

ARTICLE INFO

*Article history:*
Received 17 April 2011
Available online 28 April 2011

*Keywords:*
Actinin-associated LIM protein 3 (*PDLIM3/ALP*)
Alternative splicing
MBNL
Myotonic dystrophy
Sarcoplasmic/endoplasmic reticulum Ca-ATPase 1 (*SERCA1*)
ZASP-like motif

ABSTRACT

Myotonic dystrophy type 1 (DM1) is an autosomal dominant disorder of muscular dystrophy characterized by muscle weakness and wasting. DM1 is caused by expansion of CTG repeats in the 3′-untranslated region (3′-UTR) of *DM protein kinase* (*DMPK*) gene. Since CUG-repeat RNA transcribed from the expansion of CTG repeats traps RNA-binding proteins that regulate alternative splicing, several abnormalities of alternative splicing are detected in DM1, and the abnormal splicing of important genes results in the appearance of symptoms. In this study, we identify two abnormal splicing events for actinin-associated LIM protein 3 (*PDLIM3/ALP*) and fibronectin 1 (*FN1*) in the skeletal muscles of DM1 patients. From the analysis of the abnormal *PDLIM3* splicing, we propose that ZASP-like motif-deficient PDLIM3 causes the muscular symptoms in DM. PDLIM3 binds α-actinin 2 in the Z-discs of muscle, and the ZASP-like motif is needed for this interaction. Moreover, in adult humans, PDLIM3 expression is highest in skeletal muscles, and *PDLIM3* splicing in skeletal muscles is regulated during human development.

© 2011 Elsevier Inc. All rights reserved.

## 1. Introduction

Myotonic dystrophy (Dystrophia Myotonica; DM) is an autosomal dominant disorder and is the most common form of muscular dystrophy to affect adults [1]. Multiple systems are affected in patients with DM. The characteristic symptoms of DM are muscle hyper-excitability (myotonia), progressive muscle loss, muscle weakness, cataracts, defects in cardiac conduction, cognitive impairment, and insulin resistance [1]. Two forms of DM have been identified, DM1 and DM2. The gene that is affected in DM1 is *DM protein kinase* (*DMPK*) on chromosome 19q. This gene contains trinucleotide CTG repeats within its 3′-untranslated region (UTR) [2–4]. The expansion of this repeat triggers the pathogenesis of DM1 and, interestingly, the number of repeats is thought to correlate with symptom severity [4]. The gene that is affected in DM2 is *zinc finger protein 9* (*ZNF9*). This gene contains tetranucleotide CCTG repeats in intron 1 and, as in DM1, expansion of this repeat is believed to cause this disease [5]. There is strong evidence that the expanded repeat-containing mRNA species transcribed from the altered *DMPK* and *ZNF9* genes form foci that are retained within the nuclei of DM cells [5–7]. Since DM1 and DM2 overlap phenotypically, despite having different genetic loci, this finding suggests that the expanded repeats themselves cause DM [6].

There is evidence to suggest that the expanded CUG repeats transcribed from a mutated allele cause RNA gain-of-function effects that affect the functions of other cellular factors, leading to abnormalities in RNA splicing. The mis-spliced genes include those for chloride channel 1 (*CLCN1*), cardiac troponin T (*cTNT/TNNT2*), sarcoplasmic/endoplasmic reticulum Ca-ATPase 1 (*SERCA1*), insulin receptor (*IR*), microtubule-associated protein tau (*MAPT*), and amyloid precursor protein (*APP*) [8–13]. The splicing patterns of some of these genes are also aberrantly regulated in patients with DM2 [10,14,15]. These results suggest that certain RNA-binding proteins that regulate the pre-mRNA splicing of these genes are abnormally influenced by the mutant transcript that contains CUG/CCUG repeats [16]. The RNA-binding MBNL and CELF families of proteins have been identified, and cellular studies have demonstrated that *CLCN1*, *cTNT*, *SERCA1*, and *IR* are directly regulated by these proteins [17–20].

To determine the splicing abnormality and gene expression resulting from the expanded CUG mRNA, we used human exon arrays to compare the mRNA splicing patterns of the skeletal muscles of patients with DM1. We found remarkable perturbations of splicing, and identified more than 100 splicing events that were altered in DM1 muscles (Koebis, submitted). Among these altered splicing events, we focused on the *PDLIM3/ALP* (PDZ and LIM domain protein 3 α-actinin-associated LIM protein), PDZ and LIM domain protein 3 and the α-actinin-associated LIM proteinactinin-associated LIM protein, which binds to the spectrin repeat of α-actinin 2 *via* the PDZ domain in the Z-discs of muscles [21,22]. As Z-discs are

* Corresponding author.
*E-mail addresses:* cishiura@mail.ecc.u-tokyo.ac.jp, cc077725@mail.ecc.u-tokyo.ac.jp (S. Ishiura).

0006-291X/$ - see front matter © 2011 Elsevier Inc. All rights reserved.
doi:10.1016/j.bbrc.2011.04.106

essential for force transmission and muscle integrity [23], we hypothesized that abnormal *PDLIM3* splicing contributes to the symptoms of DM1.

We found that *PDLIM3* splicing was regulated during development and in a tissue-specific manner, and that the abnormal *PDLIM3* splicing was closely related with the altered splicing of *SERCA1* in each DM1 patient. We suspect that *PDLIM3* splicing is regulated by the same molecular mechanism that regulates *SERCA1*, and that abnormal splicing is developmentally regulated.

## 2. Materials and methods

### 2.1. Human skeletal muscle biopsies

Biopsies were obtained from the biceps brachii muscle or quadriceps femoris muscle of six DM1 patients and seven non-DM individuals without muscular disease (Supplementary Table). Of the non-DM individuals, three lacked histologic abnormalities, while four showed mild atrophy or atrophy of only the type 2 fibers. All the biopsies were stored at −80 °C. Clinically, all the DM1 patients had muscle weakness with myotonia. Four of the DM1 patients had congenital onset of the disease, and two experienced onset during childhood or adolescence. Pathologically, all the DM1 patients showed an immature fiber type or myopathic changes with variable fiber sizes. All biopsies were acquired with the informed consent of the patients.

### 2.2. RNA extraction and reverse transcription (RT)

Total RNA samples were isolated from the biopsies using TRIzol (Invitrogen, Carlsbad, CA), according to the manufacturer's protocol but without DNase treatment, and purified by phenol–chloroform extraction and isopropanol precipitation. Total RNA samples from other tissues were taken from the Human Total RNA Master Panel II (Clontech, Mountain View, CA). All total RNA samples were stored at −80 °C.

The cDNA samples were synthesized using the PrimeScript 1st Strand cDNA Synthesis Kit (TaKaRa Bio, Shiga, Japan) in a total volume of 10 μl using the oligo(dT) primers and the total RNA samples (0.5 μg for biopsies; 1.0 μg for other tissues). The cDNA of fetal skeletal muscle (BioChain, Hayward, CA) was synthesized using the total RNA sample from a male, 20-week-old donor. All the cDNA samples were stored at −20 °C.

### 2.3. Polymerase chain reaction (PCR)

PCR was performed using ExTaq DNA polymerase (TaKaRa Bio), according to the manufacturer's protocol. The primer sequences, annealing temperatures, and cycle numbers used are listed in Table 1. The following conditions were used for the PCR: initial denaturation at 96 °C for 2 min, followed by quantitative cycles (96 °C for 30 s, annealing temperature for 30 s, and 72 °C for 1 min), and a final extension step (72 °C for 5 min). The numbers of cycles were adjusted such that the amplification occurred within the logarithmic phase.

The PCR products were resolved by electrophoresis on an 8% polyacrylamide gel or a 1% agarose gel. The gels were strained with ethidium bromide and analyzed using LAS-3000 imaging system (Fujifilm, Tokyo, Japan). The intensity of the band signals was quantified using the Multigauge software (Fujifilm). The splicing percentages of *PDLIM3* were calculated as (PDLIM3b band)/(All isoform' bands), those of *SERCA1* were calculated as (SERCA1b band)/(All isoform' bands). The mean values are shown, and the *P*-values were determined using the Student's *t*-test. The correlation of the splicing percentages for *PDLIM3* and *SERCA1* for every DM1 patient is represented by the Pearson product-moment correlation coefficient. The PCR products were cloned into the pGEM-T Easy vector (Promega, Madison, WI) and sequenced.

## 3. Results

### 3.1. Aberrant splicing in patients with DM1

To identify aberrant alternative splicing in DM1, we performed RT-PCR on the biopsies of non-DM1 individuals and DM1 patients (Supplementary Table). From the exon array results, we selected the following six candidate exons (Table 1): *PDLIM3* exon 4; *FN1* exon 25 and exon 33; *PKP2* exon 6; *TTN* exon 45; and *EGLN2* exon 4. These genes are highly expressed in skeletal muscles or these exons are alternative exons. As a positive control (PC), we used *SERCA1*, which is known to undergo abnormal splicing in DM1 patients and DM1 model ($HSA^{LR}$) mice [12]. Assuming that the percentage of exon inclusion or exclusion relative to the total number of transcripts changes significantly, as for *SERCA1* exon 22, the same physiologic abnormality with abnormal splicing should occur in DM1 muscle. Using RT-PCR, we detected aberrant splicing for *PDLIM3* exon 4 (Fig. 1A and B; $P = 0.0015$) and *FN1* exon 33 (data not shown; $P = 0.0051$), as well as for *SERCA1* exon 22 (Fig. 1C;

**Table 1**
Primers used in RT-PCR.

| Gene | Accession number | Exon | DM1 isoform[a] | Primer name | Primer sequence (5′–3′) | Annealing | Cycle[b] |
|---|---|---|---|---|---|---|---|
| PDLIM3 | NM_001114107 | ex4 | Ex4 + ex5,6− | PDLIM3_ex4_Fw<br>PDLIM3_ex4_Rv | CAGCTCACCAGCTGTGTCTC<br>GAGCCATCGTCCACCATTCC | 66 °C | 27 |
| FN1 | NM_002026 | ex25 | − | FN1_ex25_Fw<br>FN1_ex25_Rv | ATGGACAGGAAAGAGATGCG<br>AAAAGTCAATGCCAGTTGGG | 66 °C | 30 |
| | | ex33 | ex33+ | FN1_ex33_Fw<br>FN1_ex33_Rv | CCTGGGAGCAAGTCTACAGC<br>TAGCATCTGTCACACGAGCC | 66 °C | 31 |
| PKP2 | NM_001005242 | ex6 | − | PKP2_ex6_Fw<br>PKP2_ex6_Rv | TCCAGGTGCTGAAGCAAACC<br>TCGCTTTTCTCCCATCAGCG | 66 °C | 32 |
| TTN | NM_003319 | ex45 | − | TTN_ex45_Fw<br>TTN_ex45_Rv | AGCACAGCCAACCTGAGTCT<br>CCGGTTCACCCTCTAAAACA | 54 °C | 31 |
| EGLN2 | NM_053046 | ex4 | − | EGLN2_ex4_Fw<br>EGLN2_ex4_Rv | CTGGGCAGCTATGTCATCAA<br>TGGACACCTTTCTGTCCTGA | 64 °C | 30 |
| SERCA1 (PC) | NM_004320 | ex22 | ex22− | SERCA1_ex22_Fw<br>SERCA1_ex22_Rv | ATCTTCAAGCTCCGGGCCCT<br>CAGCTCTGCCTGAAGATGTG | 63.5 °C | 25 |

[a] The DM1 isoform predominates in the skeletal muscles of patients with DM1.
[b] 'Cycle' refers to a quantitative cycle of RT-PCR for biopsies.

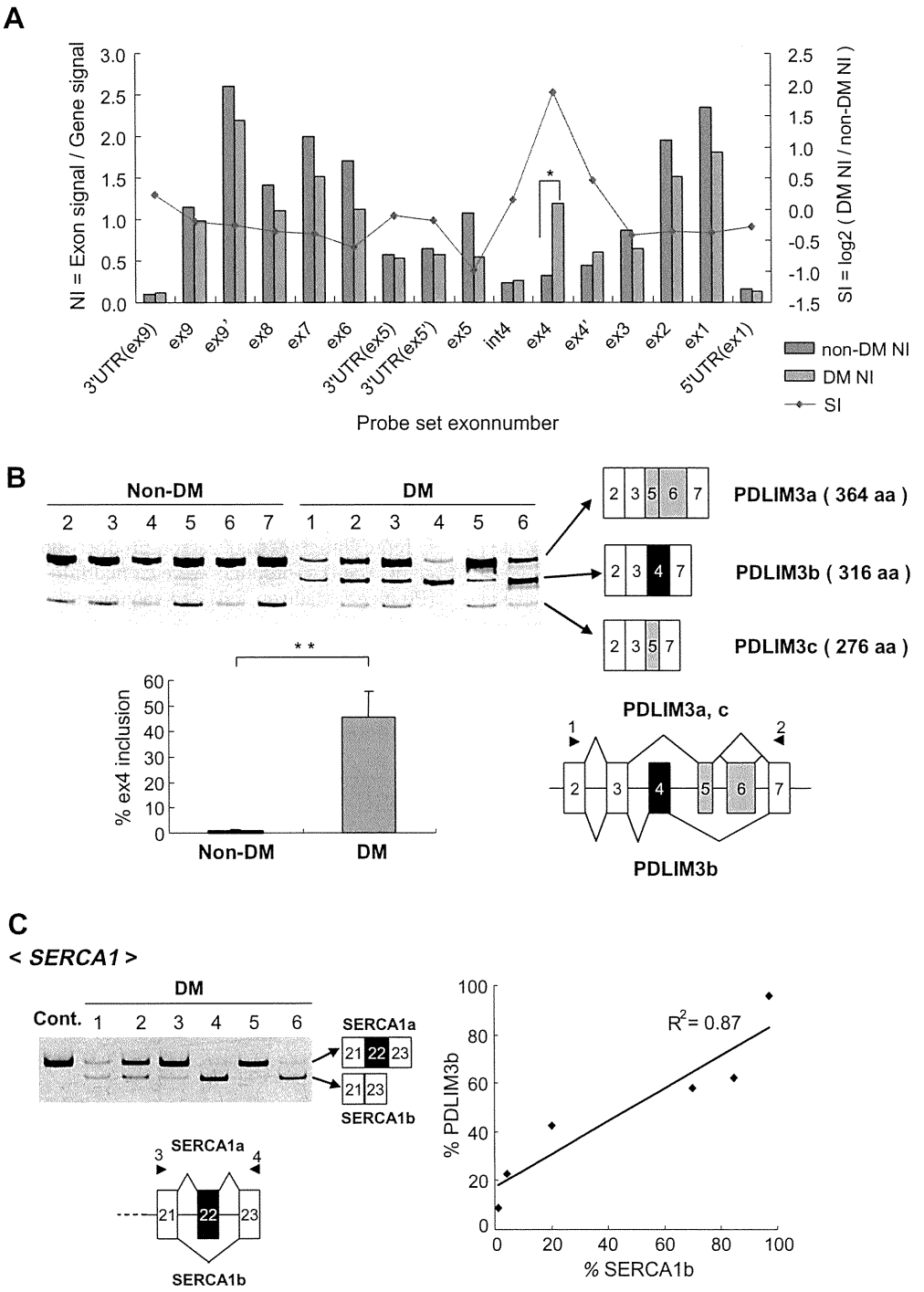


**Fig. 1.** *PDLIM3* splicing is abnormal in patients with DM1. (A) Exon array analysis of *PDLIM3* in four non-DM1 and three DM1 biopsies. NI, normalized exon intensity (NI = exon level signal/gene level signal); SI, splicing index ($SI = \log_2 NI_{DM}/NI_{non\text{-}DM}$). Statistical significance was analyzed using the Student's *t*-test for $NI_{non\text{-}DM}$ and $NI_{DM}$; $^{*}P < 0.05$. (B) The level of PDLIM3b (exon 4 inclusion isoform) is increased in DM1 muscles. RT-PCR of endogenous *PDLIM3* in DM1 skeletal muscles ($n = 6$; Nos. 1, 2, 3, 4, 5, and 6) and non-DM1's ($n = 6$; Nos. 2, 3, 4, 5, 6, and 7) was performed using the primer set (arrowhead 1, 2). The lower panel shows the percentages of exon 4 inclusion isoform relative to the total level of transcripts (means ± SD). Statistical significance was analyzed by the Student's *t*-test ($^{**}P < 0.0015$). (C) *PDLIM3* splicing correlates with *SERCA1* splicing in each DM patient. RT-PCR of endogenous *SERCA1* in DM1 skeletal muscles ($n = 6$; Nos. 1, 2, 3, 4, 5, and 6) and non-DM1 skeletal muscles (Cont.) using the primer set (arrowhead 3, 4). The right panel shows the correlation between the percentage of *PDLIM3* exon 4 inclusion isoform (% PDLIM3b) and *SERCA1* exon 22 exclusion isoform (% SERCA1b) relative to the total level of transcripts. $R^2$ is the Pearson product-moment correlation coefficient, and the correlation is significant at $R^2 > 0.87$, $P = 0.0064$.

$P = 0.022$). The remaining four exons did not show significant mis-splicing.

The three isoforms of *PDLIM3* splicing were observed. The normal isoforms are PDLIM3a ("exons 5 and 6 inclusion and exon 4 exclusion" isoform) and PDLIM3c ("exon 5 inclusion and exons 4 and 6 exclusion" isoform), which predominate in non-DM1 muscles, whereas the DM1 muscles contained the PDLIM3b isoform ("exon 4 inclusion and exons 5 and 6 exclusion" isoform). The pattern of *FN1* splicing revealed that the exon 33 exclusion isoform was more common than the exon 33 inclusion isoform in non-DM1 muscles, whereas the exon 33 inclusion isoform predominated in DM1 muscles.

To gain insight into the factors that regulate the splicing of *PDLIM3*, we compared the percentages of splicing of *SERCA1* and *PDLIM3* for each patient with DM1. *PDLIM3* splicing showed a statistically significant correlation with *SERCA1* splicing (Fig. 1C; $R^2 = 0.87$; $P = 0.0064$). However, there was also a correlation between the splicing of *SERCA1* and *FN1* ($R^2 = 0.82$; $P = 0.032$; data not shown). Nevertheless, we focused on the correlation between *PDLIM3* and *SERCA1*, since this correlation was stronger than that between *FN1* and *SERCA1*, and the expression of *PDLIM3* is high in skeletal muscles.

We considered that *PDLIM3* splicing might also be regulated by MBNL family proteins, such as MBNL1, 2, and 3, as *SERCA1* splicing is regulated by MBNL1 [19,24]. SERCA1b (exon 22 exclusion isoform) is seen in DM1 skeletal muscle and DM1 model mice: $HSA^{LR}$ [12]. During the development of fast-twitch fibers, SERCA1b is expressed in the fetal and neonatal stages but it is completely replaced by SERCA1a (exon 22 inclusion isoform) in adult muscle fibers [25,26]. Therefore, we performed a cellular splicing assay for *PDLIM3* in HEK-293, HeLa, and SH-SY5Y cells. The overexpression of MBNL1, 2, and 3 resulted in the shifting of *SERCA1* splicing from SERCA1b (exon 22 exclusion isoform) to SERCA1a (exon 22 inclusion isoform), whereas the shifting of *PDLIM3* splicing from PDLIM3b to PDLIM3a or PDLIM3c was negligible (data not shown).

Furthermore, the overexpression under the same conditions of CELF family proteins, such as CUGBP1, ETR-3, CELF3, 4, 5, and 6, showed that CUGBP1 and CELF3 increased SERCA1b (exon 22 exclusion isoform), although this result was not statistically significant. *PDLIM3* splicing was not regulated by either CUGBP1 or CELF3.

### 3.2. PDLIM3 splicing during skeletal muscle development

Using RT-PCR, we investigated whether the shift in isoforms occurred during the development of skeletal muscle (Fig. 2A). The detection of an isoform shift would indicate that *PDLIM3* splicing is regulated by factors that change according to developmental stage. In addition, this might suggest that alteration of the physiologic properties of *PDLIM3* is related to DM1 pathogenesis.

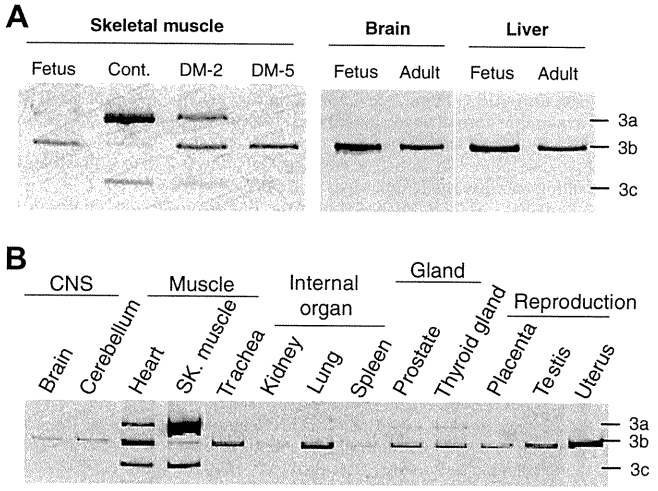


**Fig. 2.** Patterns of *PDLIM3* splicing during the development of skeletal muscles and various tissues. (A) RT-PCR of endogenous *PDLIM3* in fetal, non-DM, and DM1 skeletal muscles and other tissues. The fetal skeletal muscle isoform is PDLIM3b (exon 4 inclusion isoform), which is the same as that in the DM1 skeletal muscles (DM-2, DM-5), brain, and liver but not the same as that in the adult skeletal muscle (Cont.). PDLIM3b does not change to other isoforms during the development of the brain (fetus, 26–40 weeks; adult, 43 years old) or liver (fetus, 22–40 weeks; adult, 51 years old), except in the skeletal muscles. (B) Endogenous *PDLIM3* splicing in various tissues. The intensities of the bands obtained after 28 cycles of PCR for the exon 4 exclusion isoforms (PDLIM3a and PDLIM3c) are greater in the heart, skeletal muscle, and gland tissues. Reverse transcription of all the tissue samples was performed using 1.0 μg of total RNA.

PDLIM3b was mainly expressed in fetal skeletal muscles (Fetus; 20 weeks) (Fig. 2A), whereas PDLIM3a and PDLIM3c were predominantly detected after birth (Cont.; 6 months of age). *PDLIM3* splicing changed between 20 weeks (Fetus) and 6 months of age (infant), albeit not in the brain or liver. The change in *PDLIM3* splicing was specific for skeletal muscle. PDLIM3b was expressed mainly in DM1 skeletal muscles, but also in fetal muscles and other tissues. Thus, *PDLIM3* splicing is fetal-type in DM1, and it is thought that the condition of the DM1 muscle resembles that of fetal muscle.

To examine how *PDLIM3* splicing and expression are regulated in each tissue we performed RT-PCR on various adult tissues (Fig. 2B). *PDLIM3* splicing could be categorized into two tissue groups: muscle and other tissues. In muscle (heart and skeletal muscles), PDLIM3a and PDLIM3c were expressed predominantly, while in other tissues, the main product was PDLIM3b. In glands, low-level expression of PDLIM3a was observed. These results suggest that *PDLIM3* splicing is regulated in a muscle-specific manner. Furthermore, we detected *PDLIM3* expression in all tissues, with the exceptions of the kidneys and spleen. The level of *PDLIM3* expression was high in the heart and skeletal muscles, and low in the central nervous tissues. We conclude that *PDLIM3* expression is regulated in a muscle-specific manner.

## 4. Discussion

In the present study, we show that the splicing of *PDLIM3* exon 4 and *FN1*exon 33 occurs aberrantly in patients with DM1 (Fig. 1B). Aberrant *FN1* splicing was originally identified in patients with DM1, although it has also been reported in an array analysis of DM1 model ($MBNL^{\Delta 3/\Delta 3}$) mice [27]. The splicing changes of *FN1* have also been observed during heart development in wild-type mice [27]. Aberrant *PDLIM3* splicing has already been reported [15], although it has not been fully analyzed in patients with DM1.

In the present study, we show that *PDLIM3* splicing produces three isoforms of exons 4, 5 or 6, and that in patients with DM1, PDLIM3b ("exon 4 inclusion, exons 5 and 6 exclusion" isoform) predominates. PDLIM3 binds to α-actinin 2 via its PDZ domain [21], and the ZASP-like motif (encoded by exon 6) is necessary for this interaction [28,29]. Therefore, it is possible that the PDLIM3b proteins are unable to bind sufficiently to α-actinin 2, resulting in the symptoms of DM1 muscle. Furthermore, some mutations of *PDLIM3* have been reported in dilated cardiomyopathy (DCM) [30] and hypertrophic cardiomyopathy [31]. In addition, $PDLIM3^{-/-}$ mice develop cardiomyopathy that resembles human arrhythmogenic right ventricular cardiomyopathy (ARVD/C) with mild left ventricular involvement [32]. Therefore, *PDLIM3* may be necessary for the physiologic functions of heart muscle. However, skeletal muscle functions and development are normal in *PDLIM3*-deficient mice [22]. We propose that abnormal *PDLIM3* splicing affects the heart more than the skeletal muscles in patients with DM1.

*PDLIM3* is in the same family as *Cypher/ZASP/LDB3* [33], and abnormal *Cypher* splicing has been observed in DM1and DM2 muscles [15,34]. Moreover, *Cypher* has been linked to cardiomyopathy in mice and humans [34–36]. Moreover, *Cypher*-knockout mice die prenatally of severe congenital myopathy [34], and human *Cypher* mutations have been linked to a novel autosomal dominant muscular dystrophy [36]. Therefore, it seems that two abnormal splicings of *PDLIM3* and *Cypher* are related to the symptoms observed for DM1 muscles.

We hypothesized that *PDLIM3* splicing is regulated by MBNL family proteins, as well as *SERCA1* splicing, since a significant

correlation between *SERCA1* and *PDLIM3* splicing was detected in each patient with DM1 (Fig. 1C). However, in the cellular splicing assay, we were unable to demonstrate that MBNL or CELF family proteins regulate *PDLIM3* splicing (data not shown). In the same assay, *SERCA1* splicing was found to be regulated by MBNL. Although we carried out the splicing assay with HEK-293, HeLa, and SH-SY5Y cells, we did not detect the factors that regulate *PDLIM3* splicing. Possible reasons for this outcome are: (1) our splicing assay could not detect a minor splicing event; (2) some factor that acts with MBNL is necessary for the regulation of *PDLIM3* splicing; and (3) factors other than MBNL regulate *PDLIM3* splicing. If the amount of transfected vector that encodes each factor was increased, we might resolve issue (1) above. For issues (2) and (3), splicing factors other than MBNL might be abnormal in DM1. Currently, we are unable to conclude which of the above possibilities is the one most likely to be true.

Abnormally spliced exons in DM1 can be divided into two groups: (1) that in which the splicings become muscle-specific during development and (2) that in which the splicings change after birth [15]. *PDLIM3* exon 4 is in the former category, as the splicing pattern changed from the fetus at 20 weeks to the infant at 6 months of age (Fig. 2A). The *SERCA1* exon 22 is in the latter category [15,19]. The former group contains many gene exons that have developmental functions. Therefore, *PDLIM3* may be associated with muscle development. The developmental abnormality of *PDLIM3*$^{-/-}$ mice was observed in the heart [32], not in the skeletal muscles [22]. Moreover, *PDLIM3* may regulate muscle differentiation, since disruption of *PDLIM3* expression affects the expression of myogenin and MyoD [37].

In each human tissue, *PDLIM3* splicing was regulated in a tissue-specific manner (Fig. 2B). PDLIM3a (exon 6 inclusion isoform) was detected only in skeletal muscles and the heart. Therefore, exon 6 may have a muscle-specific function in mature muscles. As PDLIM3b (exon 4 inclusion isoform) was detected in the other tissues, exon 4 may have functions other than those it executes in skeletal muscles. Since *PDLIM3* expression was much higher in the heart and skeletal muscles than in other tissues, the roles of *PDLIM3* in other tissues may be minor.

## Acknowledgments

We would like to thank Dr. Noboru Sasagawa and Yoko Oma, Ms. Tamami Kiyatake, Zhao Yimeng, Mr. Kosuke Oana for valuable discussions. This work was supported in part by an intramural research grant (20B-13) for Neurological and Psychiatric Disorders from the NCNP, Ministry of Health, Labor and Welfare, Japan.

## Appendix A. Supplementary data

Supplementary data associated with this article can be found, in the online version, at doi:10.1016/j.bbrc.2011.04.106.

## References

[1] P. Harper, Myotonic Dystrophy, third ed., W.B. Saunders, London, 2001.

[2] J.D. Brook, M.E. McCurrach, H.G. Harley, A.J. Buckler, D. Church, H. Aburatani, K. Hunter, V.P. Stanton, J.P. Thirion, T. Hudson, et al., Molecular basis of myotonic dystrophy: expansion of a trinucleotide (CTG) repeat at the 3′ end of a transcript encoding a protein kinase family member, Cell 69 (1992) 385.

[3] Y.H. Fu, D.L. Friedman, S. Richards, J.A. Pearlman, R.A. Gibbs, A. Pizzuti, T. Ashizawa, M.B. Perryman, G. Scarlato, R.G. Fenwick Jr., et al., Decreased expression of myotonin-protein kinase messenger RNA and protein in adult form of myotonic dystrophy, Science 260 (1993) 235–238.

[4] M. Mahadevan, C. Tsilfidis, L. Sabourin, G. Shutler, C. Amemiya, G. Jansen, C. Neville, M. Narang, J. Barcelo, K. O'Hoy, et al., Myotonic dystrophy mutation: an unstable CTG repeat in the 3′ untranslated region of the gene, Science 255 (1992) 1253–1255.

[5] C.L. Liquori, K. Ricker, M.L. Moseley, J.F. Jacobsen, W. Kress, S.L. Naylor, J.W. Day, L.P. Ranum, Myotonic dystrophy type 2 caused by a CCTG expansion in intron 1 of ZNF9, Science 293 (2001) 864–867.

[6] A. Mankodi, E. Logigian, L. Callahan, C. McClain, R. White, D. Henderson, M. Krym, C.A. Thornton, Myotonic dystrophy in transgenic mice expressing an expanded CUG repeat, Science 289 (2000) 1769–1773.

[7] K.L. Taneja, M. McCurrach, M. Schalling, D. Housman, R.H. Singer, Foci of trinucleotide repeat transcripts in nuclei of myotonic dystrophy cells and tissues, J. Cell Biol. 128 (1995) 995–1002.

[8] R.N. Kanadia, K.A. Johnstone, A. Mankodi, C. Lungu, C.A. Thornton, D. Esson, A.M. Timmers, W.W. Hauswirth, M.S. Swanson, A muscleblind knockout model for myotonic dystrophy, Science 302 (2003) 1978–1980.

[9] B.N. Charlet, R.S. Savkur, G. Singh, A.V. Philips, E.A. Grice, T.A. Cooper, Loss of the muscle-specific chloride channel in type 1 myotonic dystrophy due to misregulated alternative splicing, Mol. Cell 10 (2002) 45–53.

[10] A. Mankodi, M.P. Takahashi, H. Jiang, C.L. Beck, W.J. Bowers, R.T. Moxley, S.C. Cannon, C.A. Thornton, Expanded CUG repeats trigger aberrant splicing of ClC-1 chloride channel pre-mRNA and hyperexcitability of skeletal muscle in myotonic dystrophy, Mol. Cell 10 (2002) 35–44.

[11] A.V. Philips, L.T. Timchenko, T.A. Cooper, Disruption of splicing regulated by a CUG-binding protein in myotonic dystrophy, Science 280 (1998) 737–741.

[12] T. Kimura, M. Nakamori, J.D. Lueck, P. Pouliquin, F. Aoike, H. Fujimura, R.T. Dirksen, M.P. Takahashi, A.F. Dulhunty, S. Sakoda, Altered mRNA splicing of the skeletal muscle ryanodine receptor and sarcoplasmic/endoplasmic reticulum $Ca^{2+}$-ATPase in myotonic dystrophy type 1, Hum. Mol. Genet. 14 (2005) 2189–2200.

[13] R.S. Savkur, A.V. Philips, T.A. Cooper, Aberrant regulation of insulin receptor alternative splicing is associated with insulin resistance in myotonic dystrophy, Nat. Genet. 29 (2001) 40–47.

[14] R.S. Savkur, A.V. Philips, T.A. Cooper, J.C. Dalton, M.L. Moseley, L.P. Ranum, J.W. Day, Insulin receptor splicing alteration in myotonic dystrophy type 2, Am. J. Hum. Genet. 74 (2004) 1309–1313.

[15] X. Lin, J.W. Miller, A. Mankodi, R.N. Kanadia, Y. Yuan, R.T. Moxley, M.S. Swanson, C.A. Thornton, Failure of MBNL1-dependent post-natal splicing transitions in myotonic dystrophy, Hum. Mol. Genet. 15 (2006) 2087–2097.

[16] L.P. Ranum, T.A. Cooper, RNA-mediated neuromuscular disorders, Annu. Rev. Neurosci. 29 (2006) 259–277.

[17] Y. Kino, C. Washizu, Y. Oma, H. Onishi, Y. Nezu, N. Sasagawa, N. Nukina, S. Ishiura, MBNL and CELF proteins regulate alternative splicing of the skeletal muscle chloride channel CLCN1, Nucleic Acids Res. 37 (2009) 6477–6490.

[18] T.H. Ho, B.N. Charlet, M.G. Poulos, G. Singh, M.S. Swanson, T.A. Cooper, Muscleblind proteins regulate alternative splicing, EMBO J. 23 (2004) 3103–3112.

[19] S. Hino, S. Kondo, H. Sekiya, A. Saito, S. Kanemoto, T. Murakami, K. Chihara, Y. Aoki, M. Nakamori, M.P. Takahashi, K. Imaizumi, Molecular mechanisms responsible for aberrant splicing of SERCA1 in myotonic dystrophy type 1, Hum. Mol. Genet. 16 (2007) 2834–2843.

[20] W. Dansithong, S. Paul, L. Comai, S. Reddy, MBNL1 is the primary determinant of focus formation and aberrant insulin receptor splicing in DM1, J. Biol. Chem. 280 (2005) 5773–5780.

[21] H. Xia, S.T. Winokur, W.L. Kuo, M.R. Altherr, D.S. Bredt, Actinin-associated LIM protein: identification of a domain interaction between PDZ and spectrin-like repeat motifs, J. Cell Biol. 139 (1997) 507–515.

[22] K. Jo, B. Rutten, R.C. Bunn, D.S. Bredt, Actinin-associated LIM protein-deficient mice maintain normal development and structure of skeletal muscle, Mol. Cell. Biol. 21 (2001) 1682–1687.

[23] D. Frank, C. Kuhn, H.A. Katus, N. Frey, The sarcomeric Z-disc: a nodal point in signalling and disease, J. Mol. Med. 84 (2006) 446–468.

[24] R.N. Kanadia, J. Shin, Y. Yuan, S.G. Beattie, T.M. Wheeler, C.A. Thornton, M.S. Swanson, Reversal of RNA missplicing and myotonia after muscleblind overexpression in a mouse poly(CUG) model for myotonic dystrophy, Proc. Natl. Acad. Sci. USA 103 (2006) 11748–11753.

[25] C.J. Brandl, N.M. Green, B. Korczak, D.H. MacLennan, Two $Ca^{2+}$ ATPase genes: homologies and mechanistic implications of deduced amino acid sequences, Cell 44 (1986) 597–607.

[26] C.J. Brandl, S. deLeon, D.R. Martin, D.H. MacLennan, Adult forms of the $Ca^{2+}$ATPase of sarcoplasmic reticulum. Expression in developing skeletal muscle, J. Biol. Chem. 262 (1987) 3768–3774.

[27] A. Kalsotra, X. Xiao, A.J. Ward, J.C. Castle, J.M. Johnson, C.B. Burge, T.A. Cooper, A postnatal switch of CELF and MBNL proteins reprograms alternative splicing in the developing heart, Proc. Natl. Acad. Sci. USA 105 (2008) 20333–20338.

[28] T. Klaavuniemi, A. Kelloniemi, J. Ylanne, The ZASP-like motif in actinin-associated LIM protein is required for interaction with the alpha-actinin rod and for targeting to the muscle Z-line, J. Biol. Chem. 279 (2004) 26402–26410.

[29] T. Klaavuniemi, N. Alho, P. Hotulainen, A. Kelloniemi, H. Havukainen, P. Permi, S. Mattila, J. Ylanne, Characterization of the interaction between actinin-associated LIM protein (ALP) and the rod domain of alpha-actinin, BMC Cell Biol. 10 (2009) 22.

[30] A.M. Arola, X. Sanchez, R.T. Murphy, E. Hasle, H. Li, P.M. Elliott, W.J. McKenna, J.A. Towbin, N.E. Bowles, Mutations in PDLIM3 and MYOZ1 encoding myocyte Z line proteins are infrequently found in idiopathic dilated cardiomyopathy, Mol. Genet. Metab. 90 (2007) 435–440.

[31] R.D. Bagnall, L. Yeates, C. Semsarian, Analysis of the Z-disc genes PDLIM3 and MYPN in patients with hypertrophic cardiomyopathy, Int. J. Cardiol. 145 (2010) 601–602.

[32] M. Pashmforoush, P. Pomies, K.L. Peterson, S. Kubalak, J. Ross Jr., A. Hefti, U. Aebi, M.C. Beckerle, K.R. Chien, Adult mice deficient in actinin-associated LIM-domain protein reveal a developmental pathway for right ventricular cardiomyopathy, Nat. Med. 7 (2001) 591–597.

[33] C.R. McKeown, H.F. Han, M.C. Beckerle, Molecular characterization of the *Caenorhabditis elegans* ALP/enigma gene alp-1, Dev. Dyn. 235 (2006) 530–538.

[34] Q. Zhou, P.H. Chu, C. Huang, C.F. Cheng, M.E. Martone, G. Knoll, G.D. Shelton, S. Evans, J. Chen, Ablation of Cypher, a PDZ-LIM domain Z-line protein, causes a severe form of congenital myopathy, J. Cell Biol. 155 (2001) 605–612.

[35] M. Vatta, B. Mohapatra, S. Jimenez, X. Sanchez, G. Faulkner, Z. Perles, G. Sinagra, J.H. Lin, T.M. Vu, Q. Zhou, K.R. Bowles, A. Di Lenarda, L. Schimmenti, M. Fox, M.A. Chrisco, R.T. Murphy, W. McKenna, P. Elliott, N.E. Bowles, J. Chen, G. Valle, J.A. Towbin, Mutations in Cypher/ZASP in patients with dilated cardiomyopathy and left ventricular non-compaction, J. Am. Coll. Cardiol. 42 (2003) 2014–2027.

[36] D. Selcen, A.G. Engel, Mutations in ZASP define a novel form of muscular dystrophy in humans, Ann. Neurol. 57 (2005) 269–276.

[37] P. Pomies, M. Pashmforoush, C. Vegezzi, K.R. Chien, C. Auffray, M.C. Beckerle, The cytoskeleton-associated PDZ-LIM protein, ALP, acts on serum response factor activity to regulate muscle differentiation, Mol. Biol. Cell 18 (2007) 1723–1733.

Genes to Cells

# Alternative splicing of myomesin 1 gene is aberrantly regulated in myotonic dystrophy type 1

**Michinori Koebis[1], Natsumi Ohsawa[1], Yoshihiro Kino[2], Noboru Sasagawa[3], Ichizo Nishino[4] and Shoichi Ishiura[1]***

[1]*Department of Life Sciences, Graduate School of Arts and Sciences, The University of Tokyo, 3-8-1 Komaba, Meguro-ku, Tokyo 153-8902, Japan*
[2]*Laboratory for Structural Neuropathology, RIKEN Brain Science Institute, 2-1 Hirosawa, Wako-shi, Saitama 351-0198, Japan*
[3]*Department of Applied Biochemistry, School of Engineering, Tokai University, Hiratsuka, Kanagawa 259-1292, Japan*
[4]*National Center of Neurology and Psychiatry, Kodaira, Tokyo 187-8551, Japan*

**Myotonic dystrophy type 1 (DM1) is a multisystemic disease caused by a CTG repeat expansion in the 3′-UTR of dystrophia myotonica-protein kinase. Aberrant regulation of alternative splicing is a characteristic feature of DM. Dozens of genes have been found to be abnormally spliced; however, few reported splicing abnormalities explain the phenotypes of DM1 patients. Thus, we hypothesized that other, unknown abnormal splicing events exist. Here, by using exon array, we identified aberrant inclusion of *myomesin* 1 (*MYOM1*) exon 17a as a novel splicing abnormality in DM1 muscle. A cellular splicing assay with a *MYOM1* minigene revealed that not only MBNL1-3 but also CELF1 and 2 decreased the inclusion of *MYOM1* exon 17a in HEK293T cells. Expression of expanded CUG repeat impeded MBNL1 activity but did not affect CELF1 activity on the splicing of *MYOM1* minigene. Our results suggest that the down-regulation of MBNL proteins should lead to the abnormal splicing of *MYOM1* exon 17a in DM1 muscle.**

## Introduction

Myotonic dystrophy type 1 (DM1) is an autosomal-dominant, multisystemic disease characterized by myotonia, muscle weakness, cardiac conduction deficits, insulin resistance and mental retardation (Harper 2001). DM1 is caused by an expansion of the CTG repeat in the 3′-UTR of the dystrophia myotonica-protein kinase (*DMPK*) gene on chromosome 19 (Aslanidis *et al.* 1992; Brook *et al.* 1992; Buxton *et al.* 1992; Harley *et al.* 1992), and a gain-of-function of the expanded repeat is thought to play a major role in the development of the disease (Ranum & Day 2004). Two lines of evidence supports this gain-of-function concept. First is the discovery of another type of DM, DM2. DM2 is caused by repeats at a different locus, specifically, the CCTG repeat in intron 1 of *ZNF9* on chromosome 3 (Liquori *et al.* 2001). Second is the finding that transgenic mice expressing an expanded CUG repeat driven by the human skeletal actin *HSA* promoter ($HSA^{LR}$ mice) manifest myotonia and abnormal muscle histology (Mankodi *et al.* 2000). FISH analysis revealed that transcripts with an expanded CUG/CCUG repeat exhibited foci in the nuclei of DM cells (Taneja *et al.* 1995; Davis *et al.* 1997; Liquori *et al.* 2001). It has been suggested that the abnormal behavior of the expanded CUG/CCUG repeat RNA should cause a lack of proper regulation of alternative splicing by RNA-binding proteins.

Aberrant regulation of alternative splicing is a characteristic feature of DM pathogenesis, and alternative splicing events in more than 30 genes have been found to be abnormally regulated in patients with DM (Ranum & Cooper 2006); for example, the chloride channel 1 (*CLCN1*) intron 2 and exons 6b and 7a are abnormally included in patients with DM (Charlet *et al.* 2002), and the abnormal inclusion of exon 7a from murine *Clcn1* has a clear relationship

*Communicated by*: Masayuki Yamamoto
**Correspondence*: cishiura@mail.ecc.u-tokyo.ac.jp

DOI: 10.1111/j.1365-2443.2011.01542.x
© 2011 The Authors
Journal compilation © 2011 by the Molecular Biology Society of Japan/Blackwell Publishing Ltd.

with myotonia in DM model mice (Mankodi *et al.* 2002). The aberrant splicing of multiple genes is likely to cause multisystemic symptoms in DM.

Two families of proteins, 'muscleblind-like' (MBNL) and 'CUG-BP and ETR-3-like factor' (CELF), are major candidates in the pathogenesis of DM. MBNL is a family of CCCH-type zinc finger-containing RNA-binding proteins, and three isoforms are known in human: *MBNL1*, *MBNL2/MBLL* and *MBNL3/MBXL*. Our previous study showed that all three MBNL proteins bound to CHG/CHHG repeat RNA (where H indicates A, C and U) (Kino *et al.* 2004), and MBNL1 and MBNL2 have been shown to be colocalized with CUG/CCUG inclusions in DM1 and DM2 cells (Miller *et al.* 2000; Fardaei *et al.* 2002; Holt *et al.* 2009), giving rise to an idea that MBNL function may be disrupted in DM cells. Actually, knockout of either *Mbnl1* or *Mbnl2* caused some DM-like defects in mice, such as abnormal splicing, myotonia and histological abnormalities in skeletal muscle (Kanadia *et al.* 2003; Hao *et al.* 2008), which suggests that the loss of MBNL function because of the sequestration of CUG/CCUG repeat RNA leads to the characteristic features of DM.

CUG-BP and ETR-3-like factor proteins are another family of proteins involved in the pathogenesis of DM1. CELF proteins are also a family of highly conserved RNA-binding proteins, and six genes belong to this family: CELF1/CUGBP1/CUG-BP/BRUNOL2, CELF2/ETR-3/CUGBP2/BRUNOL3, CELF3/TNRC4/BRUNOL1, CELF4/BRUNOL4, CELF5/BRUNOL5 and CELF6/BRUNOL6. Several lines of evidence has shown that CELF1 and other members of CELF family play an important role in the pathogenesis of DM. Remarkably, CELF1 is activated in DM1 cells via PKC-mediated phosphorylation (Kuyumcu-Martinez *et al.* 2007), and transgenic mice expressing human CELF1 recapitulate some of DM-like abnormalities, especially histological muscle impairment (Timchenko *et al.* 2004; Ho *et al.* 2005).

Several studies have demonstrated that both MBNL and CELF proteins directly regulate the alternative splicing dysregulated in patients with DM. Interestingly, CELF1 and MBNL1 regulate antagonistically the alternative splicing of the cardiac troponin T exon 5 and insulin receptor exon 11 (Philips *et al.* 1998; Savkur *et al.* 2001; Ho *et al.* 2004), suggesting that both the elevation of CELF1 and the loss of MBNL1 function may be involved in the development of DM. But, notably, DNA microarray analysis revealed that $HSA^{LR}$ mice and *Mbnl1*-knockout mice shared most of their splicing abnormalities: 128 of 156 abnormal splicing events in $HSA^{LR}$ mice also found in *Mbnl1*-knockouts (Du *et al.* 2010). Thus, the extent to which each of MBNL and CELF family proteins can account for splicing abnormalities and the pathogenesis of DM remains unclear.

Although splicing defects in multiple genes likely cause the multisystemic symptoms in patients with DM, no abnormal splicing event has been found to explain the development of defects in DM other than that in *CLCN1*, whose abnormal splicing may cause myotonia (Lueck *et al.* 2007). Given that the MBNL and CELF families are involved in the global shift in alternative splicing that occurs during the development of skeletal and cardiac muscle (Lin *et al.* 2006; Kalsotra *et al.* 2008), additional, unknown splicing abnormalities likely exist in DM muscle.

Searches for abnormal splicing regulation on a genome-wide scale have been conducted in several lines of model mice (Kalsotra *et al.* 2008; Du *et al.* 2010), but such comprehensive studies have rarely been performed on human patients with DM. Many efforts have been made to identify alternative splicing events that are misregulated in DM, and most studies have been based on the physiological complications of patients with DM; for example, the aberrant splicing of *CLCN1*, *IR*, sarcoplasmic/endoplasmic reticulum calcium ATPase 1 (*SERCA1*) and ryanodine receptor 1 (*RYR1*) was investigated because patients with DM show myotonia, insulin resistance and increased muscle $Ca^{2+}$ levels (Savkur *et al.* 2001; Charlet *et al.* 2002; Kimura *et al.* 2005). Thus, we investigated the comprehensive splicing profile of muscle tissue of individuals with DM1 using a splicing-sensitive microarray to identify novel aberrant splicing events in individuals with DM1. Specifically, we used the Affymetrix (Santa Clara, CA, USA) GeneChip Human Exon 1.0 ST Array. This array is a powerful tool for detecting cassette exons and mutually exclusive exons; with approximately four probes per exon, this microarray can analyze exon-level expression on a whole-genome scale.

In a comprehensive search for aberrant splicing events in patients with DM1, we found a novel splicing abnormality in *MYOM1* exon 17a. MYOM1 is a constituent of the sarcomeric M band, suggesting its involvement in muscle impairment in patients with DM. A subsequent splicing assay using a *MYOM1* minigene system revealed that MBNL and CELF family proteins function as *trans*-acting factors in the alternative splicing of *MYOM1* exon 17a. Our results


© 2011 The Authors
Journal compilation © 2011 by the Molecular Biology Society of Japan/Blackwell Publishing Ltd.

suggest that the MBNL family is a key regulator of *MYOM1* alternative splicing.

## Results

### Microarray-based comprehensive study of splicing in DM1 muscle detected novel splicing abnormalities

To investigate novel splicing defects in patients with DM1, we analyzed the splicing profiles of skeletal muscle derived from three patients with DM1 and four non-DM controls using the Human Exon 1.0 ST Array. In total, 289 probe sets displayed a significant difference (splicing index [SI] > 1 or <−1; $P < 0.05$) between the two groups, and 39 of them were designed against exons that are known or predicted to be alternatively spliced (Table S1 in Supporting Information).

### Inclusion of MYOM1 exon 17a was increased in DM1 muscle

The greatest change was recorded at exon 17a in *MYOM1* (SI = 2.47), encoding a component of the sarcomeric M band. We thus focused on this exon as a candidate whose the abnormal splicing of which might cause the muscular defects in DM and analyzed the splicing regulation of *MYOM1* exon 17a.

We confirmed the aberrant splicing of *MYOM1* exon 17a in DM1 skeletal muscle by RT-PCR (Fig. 1). Because the alternative splicing of exon 17a generates two splicing isoforms in murine embryonic heart (Agarkova *et al.* 2000), we anticipated that two isoforms (A and D in Fig. 1A) would be expressed from *MYOM1* in patients with DM1. The products amplified from isoforms A and D were expected to be 479 and 191 nucleotides in length, respectively, using the primers designed for the flanking exons (17 and 18). As in mouse skeletal muscle, isoform D was exclusively expressed in non-DM muscle (Fig. 1B). Isoform D was also dominant in DM1 muscle, but the expression of isoform A was significantly increased, in agreement with our exon array analysis. Furthermore, two additional products were amplified from the DM1 samples (Fig. 1B). Sequencing revealed that these products were isoforms of *MYOM1* containing truncated forms of exon 17a: isoform B lacked 36 nucleotides at the 3′ end of exon 17a, whereas isoform C lacked 100 nucleotides. As shown in Fig. 1D, the alternative 5′ splice sites of exon 17a used in isoform B and C are consistent with the consensus sequence of 5′ splice site.

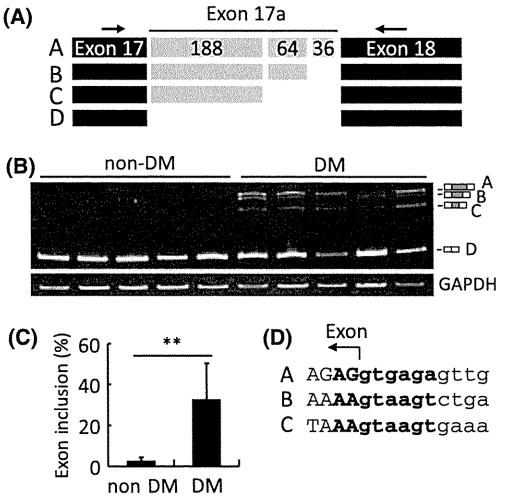


**Figure 1** The inclusion of *MYOM1* exon 17a was increased in DM. (A) Schematic diagram showing the products of the alternative splicing of *MYOM1*. The number of nucleotides of exon 17a is shown: exon 17a has two internal 5′ splice sites, generating four splicing isoforms. The names of the isoforms are given on the left side of the panel. Arrows represent the primer pairs used for RT-PCR. (B) Total RNA isolated from homogenized skeletal muscle tissue was subjected to RT-PCR and electrophoretically resolved on an 8% polyacrylamide gel. The identity of the bands is indicated on the right side of the panel. GAPDH was amplified as a loading control. (C) The histogram illustrates the inclusion of exon 17a (mean ± SD of the five individuals). The percentage of inclusions of exon 17a was calculated as the ratio of the isoforms containing full length or part of exon 17a (isoforms A, B and C) to the total spliced products. The statistical significance of the results is indicated by $^{**}P < 0.01$ (Student's *t*-test). All bands of interest were gel-isolated, cloned, and confirmed by sequencing. (D) Alternative 5′ splice sites of exon 17a.

### Both MBNL1 and CELF1 suppressed exon 17a inclusion

Next, we investigated whether MBNL and CELF family proteins regulate the splicing of *MYOM1* exon 17a using a cellular splicing assay. Because the endogenous myomesin gene was not expressed in any of the cell lines we tested, including HEK293T (see Fig. 2B, no TF), HeLa and C2C12 cells (data not shown), we constructed pMYOM1, a minigene that covered exons 17–18 of human *MYOM1* and expressed it in HEK293T cells (Fig. 2A,B). When transfected into HEK293T cells, the construct produced the same four isoforms as in DM1 muscle (Fig. 2B, vector). In HEK293T cells, 44% of the spliced product contained full length or parts of exon 17a. We then cotransfected pMYOM1 with MBNL

© 2011 The Authors
Journal compilation © 2011 by the Molecular Biology Society of Japan/Blackwell Publishing Ltd.

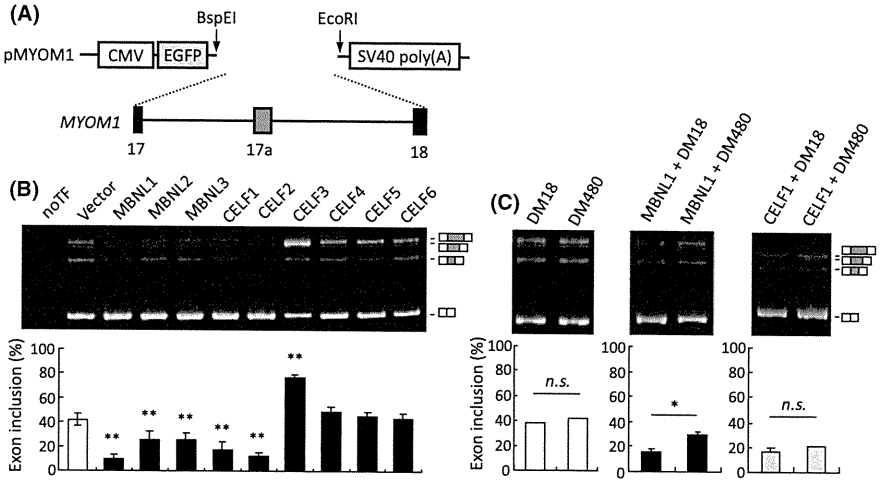


**Figure 2** CUG-BP and ETR-3-like factor and MBNL family proteins regulate *MYOM1* splicing. (A) Schematic diagram of pMYOM1 minigene. Boxes and horizontal lines represent exons and introns, respectively. The genomic region from exon 17–18 was cloned into pEGFP-C1. (B) HEK293T cells were cotransfected with the pMYOM1, and the expression vector of each protein indicated. NoTF indicates cells were transfected with pEGFP-C1 vector instead of *MYOM1* minigene. Total RNA from the cells was subjected to RT-PCR and electrophoretically resolved on an 8% polyacrylamide gel. The upper panel shows representative results of our splicing assay. All three MBNL proteins, CELF1 and CELF2 significantly repressed the inclusion of exon 17a, whereas CELF3 promoted its inclusion. The percentage of inclusion of exon 17a was calculated and shown in a histogram as in Fig. 1B ($n$ = 4). The statistical significance of the results is indicated by $^{**}P < 0.01$ (Dunnett's test). (C) The splicing regulation of MBNL1 was prevented by long CUG repeat. DM18 and DM480 indicate transfection of dystrophia myotonica-protein kinase 3′ UTR containing CUG repeat (18 and interrupted 480 repeat, respectively). The splicing pattern of pMYOM1 did not change when the minigene was cotransfected with either DM18 or DM480 in a ratio of 1:9 in HEK293T cells (left); however, when pMYOM1 was cotransfected with CUG repeat and MBNL1 in a ratio of 1:10:15, the longer CUG repeat increased the inclusion of exon 17a (middle). The splicing pattern did not change when pMYOM1 was cotransfected with CUG repeat and CELF1 (right). The inclusion rate of exon 17a was calculated and shown in a histogram as in Fig. 1B ($n$ = 3). The statistical significance of the results is indicated by $^{*}P < 0.05$ (Student's $t$-test).

and CELF family proteins and examined the patterns of minigene splicing by RT-PCR (Fig. 2B). Consistent with the current model of DM pathology, all three MBNL proteins decreased the inclusion rate of exon 17a. MBNL1 changed the splicing most, with 9.8% of the spliced product containing exon 17a. Regarding the CELF proteins, CELF1 and CELF2 promoted the exclusion of exon 17a, whereas CELF3 strongly increased its inclusion. No other CELF protein had a significant effect on exon 17a splicing. The comparable expressions of the RNA proteins were confirmed in the previous study (Kino *et al.* 2009). We conducted the minigene assay on MBNL1 and CELF1 in two other cell lines: C2C12 and HeLa (Fig. S1 in Supporting Information). The effects of MBNL1 and CELF1 in the two cell lines were the same as in HEK293T; both proteins repressed the inclusion of exon 17a of p*MYOM1*, indicating that the phenomenon was not specific to HEK293T cells.

Because CUG repeat–mediated downregulation of MBNL1 function is thought to be a major cause of aberrant splicing in DM1, we tested the effect of CUG repeat RNA on the *MYOM1* alternative splicing (Fig. 2C). Unexpectedly, there was no significant difference between DM18 and DM480, which express 3′ UTR of *DMPK* containing $(CUG)_{18}$ and interrupted $(CUG)_{480}$, respectively. Because this may be due to the relatively low endogenous expression level of MBNL1 in HEK293T cells (Sen *et al.* 2010), we examined the effect of CUG repeat RNA under cotransfection of MBNL1. In the presence of abundant MBNL1, DM480 increased the inclusion of exon 17a. It is unlikely that the effect of DM480 came out as a result of MBNL1-mediated suppression of exon 17a inclusion because DM480 did not show any significant effect under CELF1 over-expression. Thus, CUG repeat should promote the exon inclusion by preventing the function of MBNL1.

## Region around exon 17a is sufficient for MBNL1 and CELF1 regulation

Surprisingly, MBNL1 and CELF1 regulate the alternative splicing of *MYOM1* to the same direction. To


© 2011 The Authors
Journal compilation © 2011 by the Molecular Biology Society of Japan/Blackwell Publishing Ltd.

determine whether MBNL1 and CELF1 suppress the inclusion of exon 17a by the same mechanism, we explored the regions required for the splicing regulation of the two RNA-binding proteins. First, we examined the contribution of the intronic sequences using intronic deletion mutant minigenes (Δ1–Δ6, Fig. 3A). Compared with pMYOM1 minigene, some mutants altered their basal splicing patterns in HEK293T cells (Fig. 3B); for example, Δ5 mutant showed the increased inclusion of exon 17a with variant C being predominant, suggesting that the region 100–500 bp downstream of exon 17a might be important for the selection of 5′ splice site of intron 17a (data not shown). As for the regulation of MBNL1 and CELF1, any deletion mutants we tested were responsive to both proteins (Fig. 3B). Δ3–Δ6 mutants had only a 100-bp intronic fragment left at the most deleted end of the intron. Thus, for the responsiveness to MBNL1 and CELF1, at least one regulatory element should lie in the exons or their flanking 100-bp intronic regions.

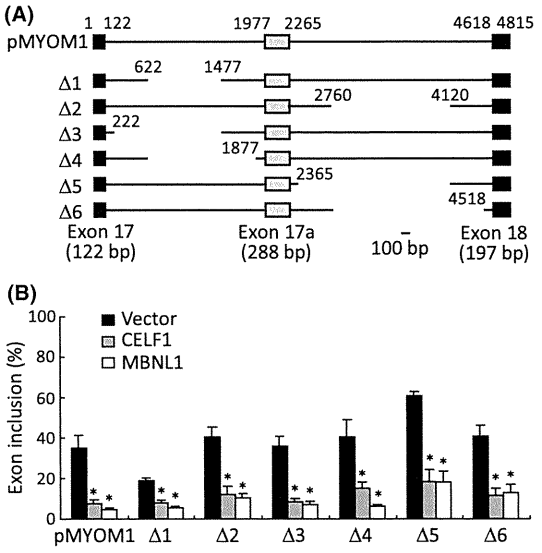


**Figure 3** Intronic deletion analysis of pMYOM1. (a) A schematic diagram showing deletion mutants. Deletion series of pMYOM1 were generated by PCR-mediated mutagenesis. The numbers indicate the positions of nucleotides at the termini of exons and the junction of deleted regions. (b) Splicing analysis of pMYOM1 deletion mutants in HEK293T cells. Deletion mutants Δ1–Δ6 were cotransfected with an empty vector, MBNL1, or CELF1 in HEK293T cells, and the inclusion of exon 17a was analyzed by RT-PCR. The percentage of inclusion of exon 17a was calculated and shown in a histogram as in Fig. 1B ($n = 4$). The statistical significance of the results is indicated by $*P < 0.05$ (Dunnett's test against vector).

We then investigated the region around exon 17a using the chimeric minigene system (Kino *et al.* 2009). In this system, we used a vector that carried a sequence covering exon 1–2 of mouse tropomyosin 2 (*Tpm2*), a gene distinct from *MYOM1* (Fig. 4A). We could insert an arbitrary exon together with its flanking introns into intron 1 of the vector; for example, we inserted *Tpm2* exon 9 as a reference (Fig. 4A, *Tpm2*-ex9). When *Tpm2*-ex9 minigene was expressed in HEK293T cells, exon 9 in intron 1 was successfully recognized as an exon, and MBNL1 hardly changed the splicing pattern of *Tpm2*-ex9 (Fig. 4B). Then, we examined a series of *Tpm2*-based chimeric minigenes that contained *MYOM1* exon 17a and its flanking introns or a hybrid of the regions around *Tpm2* exon 9 and *MYOM1* exon 17a (Fig. 4A). Like *Tpm2*-ex9 minigene, the inserted exons of these chimeric minigenes were alternatively spliced. Among the minigenes, *Tpm2*-ex17a, 17a-9 and 5′ex17a were more responsive to MBNL1 than *Tpm2*-ex9 (Fig. 4B). Because these minigenes shared 158 bp of the 5′ region of *MYOM1* exon 17a, we substituted this segment in *Tpm2*-ex17a minigene with a corresponding one of *Tpm2* exon 9. The resulting minigene, Δ5′ex17a, little changed its splicing pattern when co-expressed with MBNL1 (Fig. 4C). These data suggest that a *cis*-element for MBNL1 may be located in the former half of exon 17a.

We compared the effect of CELF1 on *Tpm2*-ex17a and *Tpm2*-ex9 minigenes (Fig. 4D). This analysis revealed that *Tpm2*-ex17a, but not *Tpm2*-ex9, was responsive to CELF1, suggesting that the regulatory element(s) for CELF1 may be in the region around *MYOM1* exon 17a.

### Mutation in MBNL1-recognition motifs extinguished the responsiveness to MBNL1

A recent report has described YGCY sequence as a MBNL1-recognition motif (Goers *et al.* 2010), which is consistent with our previous study that revealed MBNL1 bound to CHHG repeat RNA (where H indicates A, U and C) (Kino *et al.* 2004; Goers *et al.* 2010). Because several studies have shown that MBNL1 requires its recognition motif(s) in the target sequence to regulate splicing (Ho *et al.* 2004; Hino *et al.* 2007), we searched YGCY motifs in the MBNL1-responsive region of exon 17a and found four motifs with two UGCU sequences arranged in tandem (Fig. 5A). To investigate whether MBNL1 regulates the splicing of exon 17a via these motifs, we introduced mutations into each YGCY sequence. We

© 2011 The Authors
Journal compilation © 2011 by the Molecular Biology Society of Japan/Blackwell Publishing Ltd.

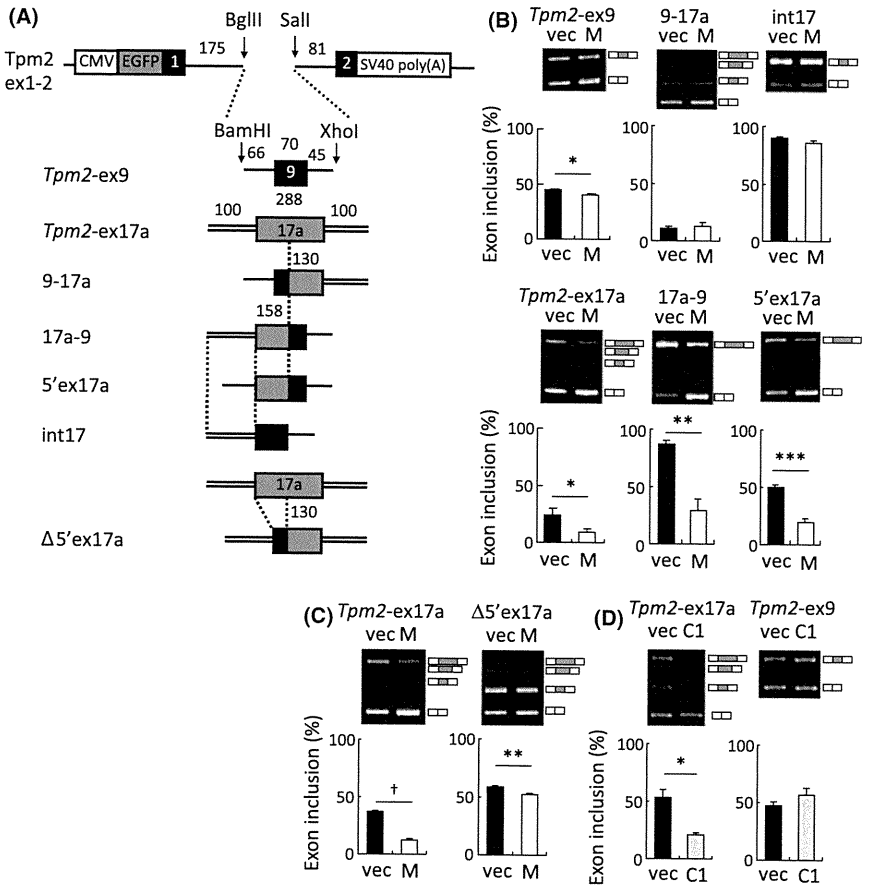


**Figure 4** Splicing regulation in chimeric minigenes. (A) Structure of the *Tpm2*-based chimeric minigene. Fragments of *Tpm2* covering exons 1–2 were inserted downstream of EGFP. Test exons together with their flanking regions were inserted into intron 1 of *Tpm2*. Intronic fragments derived from *MYOM1* are indicated by double lines, whereas those derived from *Tpm2* (regions flanking exon 9) are indicated by thin lines. Exonic sequences of *MYOM1* exon 17a and *Tpm2* exon 9 are indicated by grey and black boxes, respectively. The numbers indicate the nucleotide length of each exonic and intronic sequences. (B) Splicing assay results using *Tpm2*-based chimeric minigenes in HEK293T cells. Upper bands correspond to the spliced products containing an exon inserted between *Tpm2* exon 1 and 2. 'vec' and 'M' indicate empty vector and MBNL1, respectively. Compared with *Tpm2*-ex9, *Tpm2*-ex17a, 17a-9 and 5′ex17a minigenes exhibited evident responses to MBNL1. The percentage of inclusion of exon 17a was calculated and shown in a histogram as in Fig. 1B ($n = 3$). The statistical significance of the results is indicated by $*P < 0.05$, $**P < 0.01$, $***P < 0.001$ and $\dagger P < 0.0001$ (Student's *t*-test). (C) Splicing regulation of chimeric minigenes lacking the former half of exon 17a. Results of the splicing assay are shown as in B. The structures of minigenes are shown in A. (D) Sequence around exon 17a is sufficient for CELF1-mediated exon 17a exclusion. *Tpm2*-ex17a and *Tpm2*-ex9 minigenes were tested for their responsiveness to CELF1 (C1). The splicing assay was performed as in B, except that CELF1 was used in place of MBNL1. The responsibility to CELF1 was increased in the presence of exon 17a and its flanking introns.

mutated an additional UGCU motif in intron 17 because MBNL1 may require two or more YGCY motifs to regulate splicing by inducing and stabilizing a hairpin structure in a target RNA (Warf *et al.* 2009). When we expressed each of the mutated minigenes with or without MBNL1 in HEK293T cells, mut1 minigene showed a dramatic decrease in the responsiveness to MBNL1, whereas the other mutations did not change their splicing patterns (Fig. 5B).

CELF1 was also cotransfected with these mutated series of minigenes to discriminate the regulatory mechanism of CELF1 from that of MBNL1 (Fig. 5C). All the point-mutated minigenes retained the responsiveness to CELF1 in a comparable level (data not shown). Importantly, CELF1 decreased the inclusion of exon 17a in mut1 minigene, which lacked a *cis*-element for MBNL1. Therefore, CELF1 regulated the alternative splicing of *MYOM1* exon 17a in a distinct pathway from that of MBNL1.


© 2011 The Authors
Journal compilation © 2011 by the Molecular Biology Society of Japan/Blackwell Publishing Ltd.

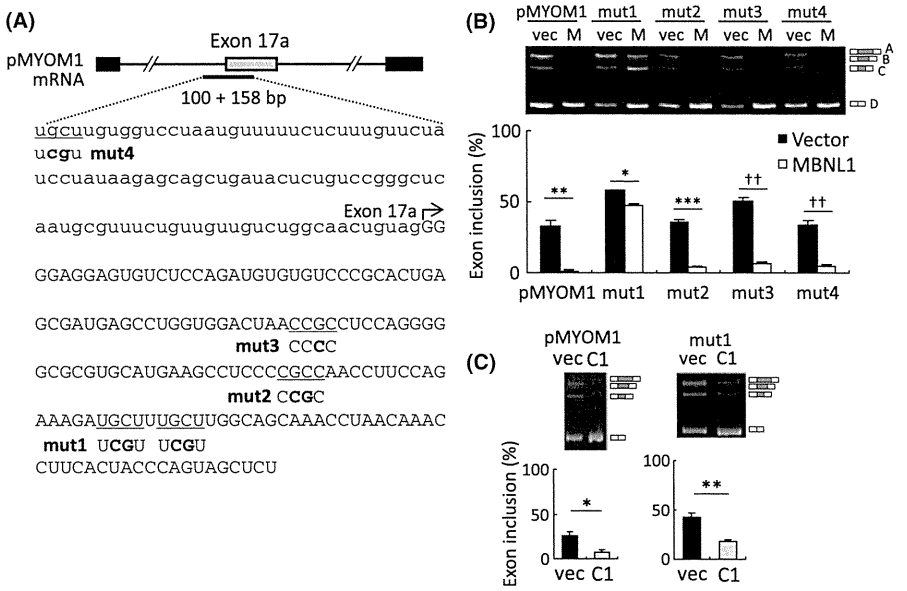


**Figure 5** Analysis of MBNL1-recognition motifs in 5′ region of exon 17a. (A) Sequence of a 158-bp portion of 5′ region of exon 17a and a 100-bp portion of its upstream intron is shown. MBNL1-recognized YGCY motifs are underlined, and sequence of a mutant minigene is shown in boldface below each motifs. (B) Result of splicing assay with mutant minigenes in HEK293T cells. The 'vec' and 'M' indicate empty vector and MBNL1, respectively. The mut1 minigene showed remarkable decrease in responsiveness to MBNL1. The percentage of inclusion of exon 17a was calculated and shown in a histogram as in Fig. 1B ($n$ = 3). (C) Same as (B) except C1 indicates CELF1. The mut1 minigene showed responsiveness to CELF1. The statistical significance of the results is indicated by $*P < 0.05$, $**P < 0.01$, $***P < 0.001$ and $††P < 0.00001$ (Student's $t$-test).

## Discussion

In this study, using splicing-sensitive microarrays, we investigated the comprehensive splicing profiles of patients with DM1 and non-DM individuals, and identified the abnormal inclusion of *MYOM1* exon 17a as a novel splicing defect in DM1. The protein encoded by *MYOM1* is a constituent of the sarcomeric M band, where it anchors the giant protein titin and maintains the thick filament lattice (Lange *et al.* 2005a,b). Like other myofibrillar proteins, MYOM1 is composed primarily of immunoglobulin-like (motif I) and fibronectin type III (motif II) domains with the arrangement II-II-I-I-I-I-I-II-II-II-II (Lange *et al.* 2005a). Exon 17a encodes a polypeptide with an EH-domain inserted between the third and fourth motif I domains; the EH-domain makes MYOM1 more elastic, like the PEVK domain in titin (Bertoncini *et al.* 2005; Schoenauer *et al.* 2005). However, the physiological importance of the inclusion of this exon is unclear. In DM1 muscle, we observed increased expression of isoform C (Fig. 1B). This isoform generates a truncated form of MYOM1 because of the presence of a premature termination codon in exon 18. Thus, the elevation of isoform C may cause a dominant negative effect and inhibit sarcomere formation in DM1 muscle. Because we focused on the regulatory mechanism of the alternative splicing of *MYOM1*, we did not study physiological significance of the finding. We are going to assess the pathological importance of the alternative splicing of *MYOM1*. Treatment of antisense oligonucleotide that prevents exon 17a inclusion is worth applying to DM model mice.

The alternative splicing of *MYOM1* exon 17a is strictly regulated in a developmental- and tissue-dependent manner: the expression of exon 17a is restricted to embryonic heart, soleus and extraocular muscle (Agarkova *et al.* 2000). Thus, the aberrant inclusion of exon 17a in DM1 muscle is consistent with other splicing abnormalities that show embryonic splicing patterns in DM1 muscle. MBNL1 regulates the developmental switch of alternative splicing in heart and skeletal muscle (Lin *et al.* 2006; Kalsotra *et al.* 2008), and the depletion of MBNL1 function is thought to play a major role in the aberrant transition of splicing to the embryonic or fetal patterns (Du *et al.* 2010). Our cellular splicing assay revealed that over-expression of MBNL family proteins decreased the inclusion of exon 17a, and the regulation of

© 2011 The Authors
Journal compilation © 2011 by the Molecular Biology Society of Japan/Blackwell Publishing Ltd.